Development of a plant carbon-nitrogen interface coupling framework in a coupled biophysical-ecosystem-biogeochemical model (SSiB5/Triffid/DayCent-SOM v1.0)

Zheng Xiang[1,2], Yongkang Xue[2*], Weidong Guo[1,4*], Melannie D. Hartman[3], Ye Liu[2,5], William J. Parton[3]

[1]School of Atmospheric Sciences, Nanjing University, Nanjing, China
[2]Department of Geography, University of California, Los Angeles, CA 90095, USA
[3]Natural Resource Ecology Laboratory, Colorado State University, CO 80523, USA
[4]Joint International Research Laboratory of Atmospheric and Earth System Sciences, Nanjing, China
[5]Pacific Northwest National Laboratory, Richland, WA 99352, USA.

Correspondence to: Yongkang Xue (yxue@geog.ucla.edu), Weidong Guo (guowd@nju.edu.cn)

Abstract. Plant and microbial nitrogen (N) dynamics and N availability regulate the photosynthetic capacity and capture, allocation, and turnover of carbon (C) in terrestrial ecosystems. Studies have shown that a wide divergence in representations of N dynamics in land surface models leads to large uncertainties in the biogeochemical cycle of the terrestrial ecosystems and then in climate simulations as well as the projections of future trajectories. In this study, a plant C-N interface coupling framework is developed and implemented in a coupled biophysical-ecosystem-biogeochemical model (SSiB5/TRIFFID/DayCent-SOM v1.0). The main concept and structure of this plant C-N framework and its coupling strategy are presented in this study. This framework takes more plant N-related processes into account. A dynamic C/N ratio for each plant functional type (PFT) is introduced to consider plant resistance and adaptation to N availability to better evaluate the plant response to N limitation. Furthermore, when available N is less than plant N demand, plant growth is restricted by a lower maximum carboxylation capacity of Rubisco (Vmax), reducing gross primary productivity (GPP). In addition, a module for plant respiration rates is introduced by adjusting the respiration with different rates at different plant components at the same N concentration. Since insufficient N can potentially give rise to lags in plant phenology, the phenological scheme is also adjusted in response to N availability. All these considerations ensure a more comprehensive incorporation of N regulations to plant growth and C cycling. This new approach has been tested systematically to assess the effects of this coupling framework and N limitation on the terrestrial carbon cycle. Long-term measurements from flux tower sites with different PFTs and global satellite-derived products are employed as references to assess these effects. The results show a general improvement with the new plant C-N coupling framework, with more consistent emergent properties, such as GPP and leaf area index (LAI), compared to the observations. The main improvements occur in tropical Africa and boreal regions, accompanied by a decrease in the bias in global GPP and LAI by 16.3% and 27.1%, respectively.

1 Introduction

Land surface processes substantially affect climate (Foley et al., 1998; Ma et al., 2013; Sellers et al., 1986; Xue et al., 2004, 2010, 2022) and are influenced by climate in turn (Bonan, 2008; Liu et al., 2019, 2020; Zhang et al., 2015), forming complex feedback loops to climate change (Friedlingstein et al., 2006; Gregory et al., 2009). To study these processes, the land surface components of Earth System Models (ESMs) have evolved from those that represent only physical processes (i.e., hydrology and the energy cycle) to those that include the terrestrial carbon (C) cycle, vegetation dynamics, and nutrient processes (Cox, 2001; Dan et al., 2020; Foley et al., 1998; Oleson et al., 2013; Sellers et al., 1996; Sitch et al., 2003; Wang et al., 2010; Zhan et al., 2003).

Current land surface models have large uncertainties in predicting historical and recent C exchanges (Beer et al., 2010; Kou-Giesbrecht et al., 2023; Richardson et al., 2012), and the dynamic vegetation models tend to overestimate terrestrial C sequestration (Anav et al., 2015; Heikkinen et al., 2021; Murray-Tortarolo et al., 2013; Oliveira et al., 2021). The uncertainty/errors in predictions using land models have been attributed to many factors. The parameterization of some processes has been criticized for being oversimplified from an ecological point of view (Ali et al., 2015; Lawrence et al., 2019; Reich et al., 2006). The inclusion or exclusion of nutrient limitations on productivity is one of the critical factors. The C-only models ignore significant nitrogen (N) impacts and therefore overestimate C sequestration by terrestrial ecosystems under climate change (Peñuelas et al., 2013; Zaehle et al., 2015). Ecosystem N cycling processes are among the dominant drivers of terrestrial C-climate interactions through their impacts, mainly N limitation, on vegetation growth and productivity (Reich et al., 2006), especially in N-poor younger soils at high latitudes (LeBauer & Treseder, 2008; Vitousek and Howarth, 1991), and on microbial decomposition of organic matter (Hu et al., 2001). As such, the N cycle and its effect on C uptake in the terrestrial biosphere have been incorporated into land surface models (LSMs) of ESMs (Davies-Barnard et al., 2020; Kou-Giesbrecht et al., 2023) with various representations of N processes (Ali et al., 2015; Asaadi et al., 2021; Ghimire et al., 2016; Goll et al., 2017; Lawrence et al., 2019; Oleson et al., 2013; Smith et al., 2014; Thum et al., 2019; Wiltshire et al., 2020).

Adequate C-N coupling in plant N processes, however, has been indicated as an area that still needs intensive investigation (Thum et al., 2019; Ghimire et al., 2016; Goll et al., 2017; Yu et al., 2020; Zaehle et al., 2015; Zhu et al., 2019). The fundamental aspects of N cycling for terrestrial biosphere models, such as N limitation of vegetation growth, strategies in which vegetation invests C to increase the N supply under N-limited conditions, and N limitation of decomposition, have been identified as important challenges for representing N cycling in terrestrial biosphere models (Meyerholt et al., 2020; Peng et al., 2020; Zaehle et al., 2015). Some key plant N processes, such as N limitation on gross primary productivity (GPP), the effect of biomass N content on autotrophic respiration, plant N uptake, ecosystem N loss, and biological N fixation, have been introduced into LSMs with various complexities to determine the effects of N limitation in current land models. These methods include, for instance, using N to scale down the photosynthesis parameter V(c, max) (Ghimire et al., 2016; Zaehle et al., 2015) or potential GPP to reflect N availability (Gerber et al., 2010; Oleson et al., 2013; Wang et al., 2010), defining the C cost of N uptake (Fisher et al., 2010a) and optimizing N allocation for leaf processes (Ali et al., 2015). The wide variety of assumptions and formulations of N cycling processes and C-N coupling reflects knowledge gaps and divergent theories, and further investigation is imperative (Kou-Giesbrecht et al., 2023). The coupling of N processes is still an area of model development. In the latest Coupled Model Intercomparison Project Phase 6 (CMIP6, Eyring et al., 2016), although there were 112 different coupled models with various land surface models from 33 research teams, only about 10 models incorporated an N cycle module (Arora et al., 2020).

This paper presents a recently developed process-based plant C-N coupling framework with a consistent coupling strategy between biophysical and biogeochemical processes. The framework mainly focuses on the effects of N limitation on plant photosynthesis (Section 2.2.3), plant respiration (Section 2.2.4), and plant phenology (Section 2.2.5) with a dynamic C/N ratio (CNR, section 2.2.2). The dynamic plant CNR is a more realistic representation than the fixed plant CNR in assessing the effect of N limitation on plant C processes and interactions between plant C and N processes. We implement this plant C-N framework by coupling a soil organic matter and nutrient cycling model (DayCent-SOM; Del Grosso et al., 2000; Parton et al., 1998, 2010)with a biophysical/dynamic vegetation model (SSiB5/TRIFFID, the Simplified Simple Biosphere Model version 5/Top-down Representation of Interactive Foliage and Flora Including Dynamics Model, Cox, 2001; Harper et al., 2016; Liu et al., 2019; Xue et al., 1991; Zhan et al., 2003; Zhang et al., 2015). The SSiB and TRIFFID have been extensively used for the land-atmosphere interaction studies (Harper et al., 2016; Xue et al., 2004, 2010, 2022, 2023). DayCent-SOM, which includes only the soil organic matter (SOM) cycling and trace gas subroutines from the DayCent ecosystem model (Parton et al., 1998, 2010), represents SOM transformations, below-ground N cycling, soil N limitation to microbial processes and plant growth, and nitrification/denitrification processes. In the coupled model, the potential N uptake depends on plant N demand from a biophysical and dynamic vegetation model, SSiB5/TRIFFID. The actual plant N uptake is limited based on soil N availability, as predicted by DayCent-SOM (Del Grosso et al., 2000; Parton et al., 1998, 2010). Although this plant C-N coupling framework is developed based on SSiB5, TRIFFID, and DayCent-SOM, the methodology and approach in this study could be applied to other process-based land models with similar physical, biological, and ecological principles. The coupled model is verified at thirteen flux tower sites (Lund et al., 2012; Pastorello et al., 2020) with different plant functional types (PFTs) and is used to conduct several sets of global 2-D offline simulations from 1948 to 2007 to assess the effects of the coupling process. Model predictions of global GPP and LAI have been evaluated against satellite-derived observational data(Jung et al., 2009; Sheffield et al., 2006; Zhu et al., 2013). The results demonstrate the relative importance of different plant N processes in this C-N framework.

The model used in this paper is presented in section 2.1. The development and implementation of this plant C-N framework are presented in section 2.2. The model forcing and validation data used in this paper are presented in section 2.3. In section 3, the experimental design is described. In section 4, the measurements from the flux tower sites with different PFTs and the global satellite-derived observations from 1982-2007 are used as references to assess the effect of the C-N coupling process on the long-term mean vegetation distribution using the offline SSiB5/TRIFFID/DayCent-SOM. Some issues and conclusions are presented in section 5.

2 Methods

2.1 Model description

2.1.1 SSiB4/TRIFFID model

The Simplified Simple Biosphere Model (SSiB, Xue et al., 1991; Sun and Xue, 2001; Zhan et al., 2003) is a biophysical model that simulates fluxes of surface radiation, momentum, sensible heat, and latent heat, as well as runoff, soil moisture, surface temperatures, and vegetation GPP, based on energy and water balance and photosynthesis processes. The SSiB was coupled with a dynamic vegetation model, the Top-down Representation of Interactive Foliage and Flora Including Dynamics Model (TRIFFID), to calculate net primary productivity (NPP), leaf area index (LAI), canopy height, and PFT fractional coverage according to the C balance (Cox, 2001; Harper et al., 2016; Liu et al., 2019; Zhang et al., 2015). Moreover, the surface albedo and aerodynamic resistances are also updated based on the vegetation LAI, vegetation cover, vegetation height, and greenness. Previous work has improved the PFT competition strategy and plant physiology processes to make the SSiB4/TRIFFID suitable for seasonal, interannual, and decadal studies (Zhang et al., 2015). SSiB4/TRIFFID includes seven PFTs: (1) broadleaf evergreen trees (BET), (2) needleleaf evergreen trees (NET), (3) broadleaf deciduous trees (BDT), (4) C3 grasses, (5) C4 plants, (6) shrubs, and (7) tundra. PFT coverage is determined by NPP, competition between species, and disturbance, which includes mortality due to fires, pests, and windthrow. A detailed description and validation of SSiB4/TRIFFID can be found in Zhang et al. (2015), Liu et al. (2019), and Huang et al. (2020). In this study, DayCent-SOM (see the next section) is introduced and coupled with SSiB5/TRIFFID using the C-N interface coupling framework introduced in this study, which will be discussed in section 2.2.

2.1.2 DayCent-SOM model

DayCent-SOM, a subset of DayCent that excludes plant growth, soil hydrology, and soil temperature subroutines, consists of soil mineral N pools (ammonium and nitrate) and six types of organic C and N pools consisting of two non-woody plant litter pools (metabolic and structural), three coarse woody debris pools (from the death of large wood, fine branches, and coarse roots), and three kinetically defined organic matter pools (active, slow, and passive); all types of organic pools except the passive pool have both aboveground and belowground counterparts (Table 1). Non-woody plant litter is partitioned into structural (lignin + cellulose) and metabolic (labile) litter based on the lignin: N ratio of the plant material (Parton et al., 1994). The coarse woody debris pools decay in the same way that the structural pool decomposes, with lignin and cellulose going to the slow soil organic matter pool and the labile fraction going to the active soil organic matter pool. Each type of organic pool has its own intrinsic rate of decomposition, which is modified by temperature and moisture (Parton et al., 1994). Additionally, the decomposition rates of the structural material and coarse woody debris pools are functions of their respective lignin fractions. DayCent's litter decay model has been validated using extensive data from LIDET litter decay experiments from all over the world (Bonan et al., 2013).

Table 1. The Nitrogen Pools in DayCent-SOM

		Aboveground	**Belowground**
Mineral N pool			Soil mineral N pools
Organic N pool	non-woody litter pools	Surface structural N Surface metabolic N	Soil structural N Soil metabolic N
	woody debris pool	Surface dead N	
	kinetically defined organic matter pools	Surface active N Surface slow organic N	Soil active organic N Soil slow organic N Soil passive organic N

2.2 Development of a plant carbon–nitrogen (C–N) interface coupling framework

2.2.1 Conceptual considerations and coupling strategy

To represent C and N interactions, we develop a plant C-N interface framework to couple biophysical and biogeochemical processes in the terrestrial C and N cycles. In this study, we applied the coupling framework to SSiB5/TRIFFID/DayCent-SOM. The conceptual considerations in developing this framework are presented in this section. For a process-based model, introducing a consistent coupling philosophy between biophysical and biogeochemical processes is necessary. The surface water, radiation, carbon fluxes, and plant litter are calculated by SSiB5/TRIFFID. The soil N dynamics model (DayCent-SOM) is directly driven by soil temperature, soil moisture, net radiation and plant C and N litter inputs into the soil organic pool, which are provided by the SSiB5/TRIFFID. DayCent-SOM then computes daily changes in all organic matter and mineral soil pools, estimates losses of N from nitrate leaching and N_2O, NO_x, and N_2 emissions, predicts the amount of inorganic N available to plants, and updates inorganic N pools after accounting for plant N uptake by SSiB5/TRIFFID. Following plant N uptake from DayCent-SOM, our plant C-N interface framework describes the effects of N on photosynthesis, plant autotrophic respiration, and plant phenology (Fig. 1). All these effects are associated with a dynamic CNR. In the original land surface model (SSiB4/TRIFFID), with assumed unlimited N availability and fixed CNR based on PFT, the assimilated C determined the N contents of leaves, stems, and roots, which influenced photosynthesis, autotrophic respiration, NPP, and LAI. However, more evidence indicates that the CNR is not fixed in plant life, which will be further discussed in section 2.2.2. With the dynamic CNR, the effect of N limitation on Rubisco capacity and photosynthesis is assessed (section 2.2.3).

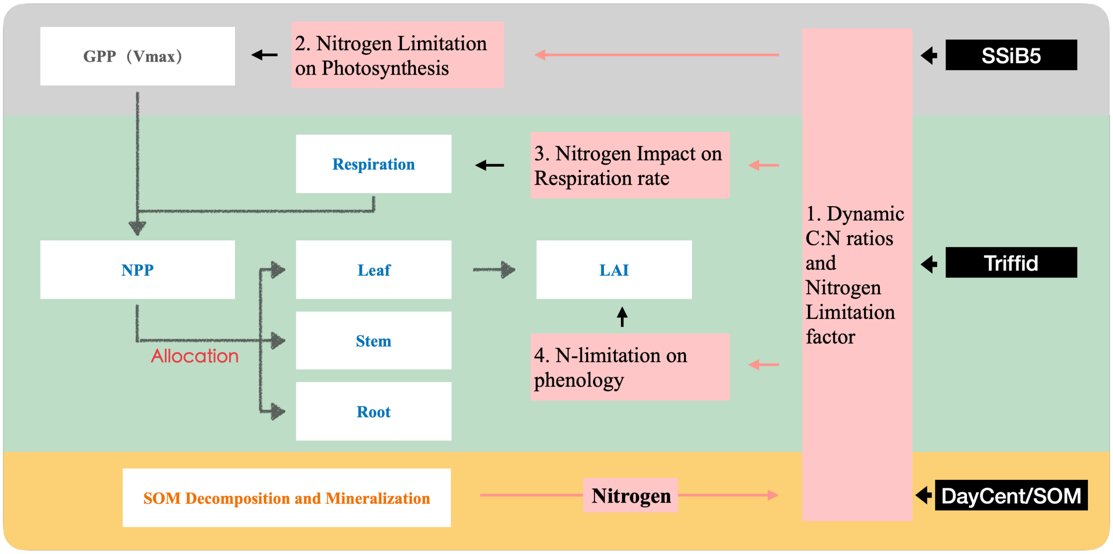

Figure 1. Schematic diagram of plant biogeochemistry and nitrogen impacts in SSiB5/TRIFFID/DayCent-SOM.
Notes: (1) Different background colors represent three different modules: SSiB, TRIFFID, and DayCent/SOM; (2) White boxes indicate the main processes involved in C-N coupling in different modules; (3) Vermeil boxes indicate how nitrogen influences plant biogeochemistry through the C-N framework.

Moreover, nitrogen is not the only dominant regulator of photosynthesis and vegetation dynamics. Reich et al., (2008) demonstrated strong relationships between respiration and N limitation based on observational data from various species. In the common N concentration range, respiration rates are consistently lower on average in leaves than in stems or roots. Therefore, this framework introduces two parameters for stems and roots based on PFT and available N, respectively, to adjust the respiration rate (section 2.2.4). Furthermore, N also affects plant phenology and can be remobilized to supply spring bud break or vegetative shoot extension (Cox, 2001; Kolb and Evans, 2002; Marmann et al., 1997; Millard, 1994; Neilsen et al., 1997). The framework includes the impact of N on plant phenology by introducing an N limitation parameter, which will be discussed in section 2.2.5. With consideration of the effect on phenology, the N limitation effect during the growth season is emphasized. All these considerations in the framework should help to understand the effects of N processes to the C cycle more comprehensively

2.2.2 Dynamic C/N ratio based on plant growth and soil nitrogen storage

Plants often face significant challenges in obtaining an adequate supply of nutrients to meet the demands of basic cellular processes. Nutrient deficiency may result in decreased plant productivity and/or plant fertility(McDowell et al., 2008; Morgan and Connolly, 2013; Stenberg and Muola, 2017). Evidence has shown that plant CNR can change with nutrient availability (Chen and Chen, 2021; McGroddy et al., 2004; Meyer-Grünefeldt et al., 2015; Sardans et al., 2012; Smith, 1991). Plant cell CNRs are influenced by the accumulation of C polymers, such as carbohydrates, and are greater when cells are nutrient starved or exposed to high levels of photosynthetically active radiation (PAR) (Aber et al., 2003; MacDonald et al., 2002; Talmy et al., 2014). The studies of ecological stoichiometry (Sterner and Elser, 2002), which investigates how the availability of multiple elements, including carbon, nitrogen, and phosphorus, constrains ecological interactions, have revealed that plants respond and adapt to lower N availability. Studies show that plants resorb only about 50% of leaf N on average (Aerts, 1996) to conserve nutrients (Clarkson and Hanson, 1980) and to increase nutrient use efficiency (Herbert and Fownes, 1999; Vitousek, 1982). These processes cause changes in the CNR to reduce the impact of N limitation (Talhelm et al., 2011; Vicca et al., 2012).

For the response of vegetation to N limitation, i.e., the strategies in which vegetation invests C to increase N supply under N-limited conditions, some models represent flexible C/N stoichiometry, while others represent time-invariant C/N stoichiometry (Kou-Giesbrecht et al., 2023). Importantly, flexible vs. time-invariant C/N stoichiometry determines terrestrial C storage per unit N, followed by plant C allocation and partitioning. Plant responses are limited under a fixed CNR, which affects plant productivity and litter N content, thus affecting underground biogeochemistry and ultimately C and N uptake and storage. Comparing field measurements, it was found that allowing adaptations in the stoichiometry of C and N helped the land model improve the terrestrial surface C and N cycle simulation(Drewniak and Gonzalez-Meler, 2017; Medlyn et al., 2015).

In this study, dynamic CNRs are introduced into SSiB5/TRIFFID. This dynamic CNR can enable vegetation to increase N uptake under N-limited conditions, reduce N limitation, and sustain terrestrial C sequestration. Plant resistance and adaptation to N availability (N_{avail}) are represented by dynamic CNRs in SSiB5. The N availability (N_{avail}) for new growth limits the C assimilation rate through the CNRs, i.e., the model-simulated NPP should be no more than the $N_{avail} \times$ CNR of new plant material. In the original TRIFFID parameterization, the CNRs for different plant components (leaf, root, and stem) are fixed based on plant functional types (Cox, 2001), and the change in CNR that occurs over the ecological process and varies with nutrient availability was not considered. A relationship between the CNR and N_{avail}, based on DayCent's parameterization, is introduced to the SSiB5/TRIFFID/DayCent-SOM for each PFT component (Fig. 2, Eq. 1).

$$CNR = \begin{cases} CNR_{max}, & N_{avail} \leq N_{min} \\ \frac{N_{avail}-N_{,max}}{N_{min}-N_{max}} \times CNR_{min} + \frac{N_{avail}-N_{min}}{N_{max}-N_{min}} \times CNR_{max} & N_{min} < N_{avail} < N_{max} \\ CNR_{min}, & N_{avail} \geq N_{max} \end{cases} \tag{1}$$

where N_{avail} is the amount of soil mineral nitrogen that was available at the end of the previous day (g N m^{-2}) calculated from DayCent-SOM.

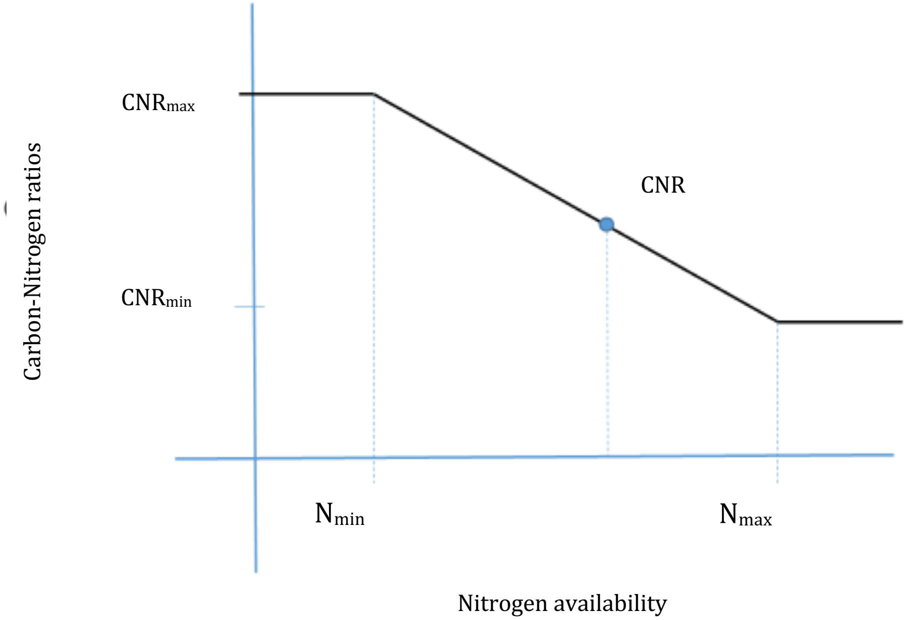

Figure 2. The relationship between soil nitrogen availability and plant carbon-nitrogen ratios.

The minimum and maximum amounts of nitrogen (N_{min}, N_{max}) necessary for the potential NPP_p (g C m^{-2} day^{-1}), which is first calculated from the SSiB5/TRIFFID with unlimited N, are:

$$N_{min} = \frac{NPP_p}{CNR_{max}} \tag{2}$$

$$N_{max} = \frac{NPP_p}{CNR_{min}} \tag{3}$$

where CNR_{min} and CNR_{max} are the minimum and maximum CNRs, respectively, for each PFT component from DayCent (Table 2). Allometric relations and empirical datasets are used to constrain the range of possible CNRs. The CNRs of leaves, fine roots, and stems were obtained from DayCent's user manual and other published papers (Parton et al., 1993, 2007). Note that Eq. (2) and Eq. (3) are calculated based on the potential NPP; the CNR that is calculated based on Eqs. 1-3 ensures that when N_{avail} varies between N_{min} and N_{max} , the plant can adjust the CNR to support this potential NPP (as demonstrated in the schematic diagram in Figure 2). That said, N limitation will have no effect on C assimilation as long as N_{avail} is greater than N_{min}. However, the N content of plant litter falling to the soil was determined by this dynamic CNR. Compared with the constant CNR, the range of possible plant carbon variation with dynamic CNR is smaller, reducing the impact of N limitation. As reviewed at the beginning of this section, a number of recent studies have demonstrated that allowing adaptations in the stoichiometry of C and N would improve plant responses; for instance, an increase in available foliar N decreases the CNR in leaves, driving an increase in productivity.

Table 2. C-N ranges of leaves, fine roots, and stems for each plant function type (PFT).

	Plant component	CNR_{min}	CNR_{max}
Broadleaf deciduous	Leaves	20	50
	Roots	40	70
	Stems	200	500
Broadleaf Evergreen	Leaves	20	40
	Roots	40	70
	Stems	150	300
Needleleaf Evergreen	Leaves	30	60
	Roots	40	60
	Stems	400	800
C3 grass	Leaves	20	40
	Roots	40	50
	Stems	40	80
C4 plants	Leaves	20	60
	Roots	60	100
	Stem	60	100
shrub	Leaves	20	40
	Roots	40	70
	Stems	200	400
tundra	Leaves	20	40
	Roots	40	80
	Stems	300	700

Note: The CNR_{min} and CNR_{max} data for each PFT component are from DayCent's user manual and other publications (Parton et al., 1993, 2007)

The DayCent-SOM only provides the total available nitrogen (N_{avail}) for the plant within one grid box (the soil is 3.2 m in depth), which consists of several PFTs. To apply equation 1, the nitrogen available for each PFT and its plant components in the grid box is calculated as

$$N_{avail}(\mathrm{i}) = N_{avail} * frac_i \quad (4)$$

$$N_{avail}(\mathrm{i},\mathrm{j}) = N_{avail}(\mathrm{i}) * \Delta \mathrm{C_j} / \Sigma_\mathrm{j} \Delta \mathrm{C_j} \quad (5)$$

where $frac_i$ is the fraction of PFT i in one grid, and ΔCj is the fraction of carbon allocated to plant component j, which consists of leaves, roots, and stems and is calculated in TRIFFID.

Furthermore, the dynamic CNR in this framework depends on the degree to which the N demands of different plant components (e.g., leaves, roots, and stems) have been satisfied over the past several days, and Eq. 1 prevents unrealistic instantaneous downregulation of potential photosynthesis rates. "Instantaneous downregulation" refers to the fact that photosynthesis rates are limited as soon as N (either in leaves or soil) is not sufficient (Reich et al., 2006; Ghimire et al., 2016), which has been applied in some N-limited models (Davies-Barnard et al., 2020). In our framework, by adjusting C/N ratios, the N limitation effect under certain conditions does not instantaneously respond to available N. The N limitation will produce effects only when available N passes some critical value (see further discussions in section 2.2.3).

2.2.3 Effect of nitrogen limitation on photosynthesis based on soil available nitrogen and the plant C/N ratio

The widely used parameterization of photosynthetic C assimilation by the terrestrial biosphere in ESMs, including our model, is represented by the Farquhar, von Caemmerer, and Berry (FvCB) model of photosynthesis (Collatz et al., 1991; Farquhar et al., 1980). At high levels of PAR, the photosynthetic rate is limited by the amount of Rubisco in the leaf and its cycling rate. Nitrogen is an important constituent of the Rubisco enzyme and mitochondrial enzymes that regulate respiration and adenosine triphosphate (ATP) generation (Makino and Osmond, 1991). As one of the most important photosynthetic model parameters, the maximum carboxylation rate by the Rubisco enzyme ($\mathrm{V_{c,max}}$) is a key parameter in the FvCB model (Farquhar et al., 1980) and has an extensive range across the models depending on the plant N content (Rogers, 2014). Therefore, leaf N content will affect $\mathrm{V_{c,max}}$ and thus GPP. However, the original FvCB model did not explicitly consider the effect of N on photosynthesis. While N limitation was introduced to terrestrial biosphere models, they differ in how N limitation in the plant C process is represented (Thomas et al., 2015; Fisher et al., 2010b). In a number of LSMs, an empirical relationship is applied to relate $\mathrm{V_{c,max}}$ to leaf N content $\mathrm{N_{leaf}}$ to determine the effect of N on photosynthesis, e.g., $\mathrm{V_{c,max}} = \mathrm{i_v} + \mathrm{s_v} \times \mathrm{N_{leaf}}$, where the intercept ($\mathrm{i_v}$) and slope ($\mathrm{s_v}$) are derived for each PFT based on observations (Kattge et al., 2009; Raddatz et al., 2007). Some studies applied the same N limitation factor to NPP or GPP (Ali et al., 2015; Fisher et al., 2010; Ghimire et al., 2016). If NPP is adjusted, the same N limitation for photosynthesis is applied for plant respiration, which is not reasonable based on plant physiology (Högberg et al., 2017). Such approaches may distort the ratio of NPP and respiration. On the other hand, if only the GPP is adjusted for N limitation, then the N limitation for respiration is ignored.

We chose the most physiological method by adjusting the maximum Rubisco carboxylation rate ($V_{c,\mathrm{max}}$), which is proportional to the nitrogen content of the Rubisco leaf reserve) during photosynthesis rather than adjusting the NPP at the end of photosynthesis. $V_{c,max}$ regulates both C assimilation and autotrophic respiration, and the photosynthesis assimilation product, GPP, is proportional to $V_{c,max}$,. Empirical evidence has shown that $V_{c,max}$ decreases with decreasing leaf N (Walker et al., 2014). We therefore introduce a downregulation of the canopy photosynthetic rate based on the available mineral N for new growth (N_{avail}) using the N availability factor $f(N)$.

$$V_{c,max,Nlimit} = V_{c,max} * f(N) \tag{6}$$

The $f(N)$ is determined by nitrogen availability:

$$f(N) = \begin{cases} \frac{N_{avail}}{N_{min}} & N_{avail} \le N_{min} \\ 1 & otherwise \end{cases} \tag{7}$$

Because plants can adjust the relative allocations of C and N during N uptake via N remobilization and resorption to reduce the impact of N limitation, as discussed in the previous section for dynamic CNR, the N limitation effect on photosynthesis only applies when nitrogen availability is lower than the minimum amount of nitrogen (N_{min}) necessary for the potential NPP. We take into account the fact that plant responses include resistance and adaptation through this approach along with the dynamic CNR to make the N-limiting effect neither linear nor instantaneously downregulate the available N content, as discussed in the last section. A linear relationship between $f(N)$ and N_{avail} is valid only when N availability is not sufficient for the minimum N demand for new growth.

2.2.4 Improvement in the impact of nitrogen on respiration rates based on field observations

Based on a database (Reich et al., 2008) of 2510 measurements from 287 species, the relationships between the mass-based dark respiration rate and nitrogen concentration of leaves, stems and roots were assessed. The results indicate strong respiration–nitrogen scaling relationships for all observations and for data averaged by species. At usual N concentrations, respiration rates are consistently lower on average in leaves than in stems or roots. In the original SSiB4/TRIFFID, the total maintenance respiration (R_{pm}) is given by Cox (2001):

$$R_{pm} = 0.012 R_{dc} \frac{N_l + N_s + N_r}{N_l} \tag{9}$$

where R_{dc} is canopy dark respiration and is linearly dependent on $V_{c,max}$. The introduced N limitation of $V_{c,max}$ in section 2.2.3 also influences the effect of N on maintenance respiration. N_l, N_s and N_r are the N contents of the leaf, stem, and root, respectively, and the factor of 0.012 is from the unit conversion. Eq. (9) assumes that the respiration rates in roots and stems have the same dependence on the N content as that in leaves.

Based on the information derived from field measurements for different PFTs (Reich et al., 2008; Wang et l., 2006; Yang et al., 1992), we introduce two PFT-specific parameters ($ResA_S$, $ResA_R$) to adjust root and stem respiration. Their values are listed in Table 3.

$$R_{pm,Nlimit} = 0.012 R_{dc} \frac{N_l + ResA_S * N_s + ResA_R * N_r}{N_l} \tag{10}$$

Table 3. The values of $\boldsymbol{ResA_S}$ and $\boldsymbol{ResA_R}$ for each plant function type (PFT).

PFT	Broadleaf deciduous	Broadleaf Evergreen	Needleleaf Evergreen	C3 grass	C4 plants	shrub	tundra
$ResA_S$	1.36	1.36	1.44	1.0	1.0	1.25	1.25
$ResA_R$	1.72	1.72	1.95	1.3	1.3	1.40	1.40

Since $ResA_S$ and $ResA_R$ are generally larger than 1, new R_{pm} is larger than the original one, and the increased respiration due to the nitrogen limitation will decrease the NPP.

2.2.5 Effect of N limitation on the LAI based on plant phenology

Nutrient availability affects vegetation activity and thus plant phenology (May and Killingbeck, 1992; Millard, 1994; Neilsen et al., 1997; Piao et al., 2019; Thomas et al., 2015; Vitasse et al., 2021; Zhou et al., 2022). Studies have demonstrated that variations in nitrogen availability could change the spring and fall phenology, such as spring bud break or vegetative shoot extension (Yang et al., 2016; Yin et al., 2017; Fu et al., 2019), as well as the length of the growing season (Wang and Tang, 2019; Zhou et al., 2022). Increased soil nitrogen availability could supplement nutrient deficiencies and thus stimulate plant growth under low temperatures in early fall (Luke McCormack et al., 2014; Delpierre et al., 2016; Yin et al., 2017) and delay the end of the growing season (Wingler et al., 2006).

In TRIFFID, the leaf mortality rate and a leaf phenology parameter, p, (Cox, 2001), are introduced to represent the vegetation's phenological status (Eqs. 11 and 12) and to adjust the model-simulated seasonal maximum possible leaf area index ($LAI_{balance}$), which is based on surface carbon balance (Cox, 2001; Enquist et al, 1998), to determine the actual LAI and produce realistic phenology.

$$LAI = p \times LAI_{balance} \tag{11}$$

$$\frac{dp}{dt} = \begin{cases} -\gamma_p & \gamma_{lm} > 2\gamma_0 \\ \gamma_p(1-p) & \gamma_{lm} \le 2\gamma_0 \end{cases} \tag{12}$$

where the leaf constant absolute drop rate $\gamma_p = 20\ yr^{-1}$, the leaf mortality rate γ_{lm} is a function of temperature T (Cox, 2001), and the minimum leaf turnover rate $\gamma_0 = 0.25$ (Cox, 2001). This phenology in SSiB4/TRIFFID modulates LAI seasonal evolution, which considers leaf mortality and the temperature threshold for leaf drop, but it is not directly linked to N. The phenology parameter p indicates that "full leaf" is approached asymptotically during the growing season, and p is reduced at a constant absolute rate when the mortality rate is greater than a certain threshold value. Otherwise, p increases, but the rate of increase decreases as the growing season progresses.

Since different N states and supplies affect phenology, as discussed above, this framework includes the impact of N on plant phenology by introducing N limitation in SSiB5/TRIFFID/DayCent-SOM to take into account the effects of N on phenology. We assume that p is limited by N availability, with the new nitrogen limitation $p_{N\ Limit}$ determined by

$$p_{N\ Limit} = f(N) \times p \tag{13}$$

where $f(N)$ is calculated as described in section 2.2.3.

2.2.6 The computational flow of SSiB5/TRIFFID/DayCent-SOM

In SSiB5/TRIFFID/DayCent-SOM, SSiB5 provides GPP, autotrophic respiration, and other physical variables, such as canopy and soil temperatures and soil moisture, every 3 hours for TRIFFID (Fig. 3). The TRIFFID accumulates the GPP from SSiB5 and produces biotic C, PFT fractional coverage, vegetation height, and LAI every ten days, which are used to update surface properties in SSiB5, such as albedo, surface roughness length, and aerodynamic and canopy resistances. The plant C-N framework uses meteorological forcings (i.e., air temperature, humidity, wind, radiation, and precipitation) and physical variables (i.e., soil moisture and soil temperature) provided by SSiB5 every 3 hours and biophysical properties (vegetation fraction and biotic C) provided by TRIFFID, which are updated every ten days. The plant C-N interface framework calculates the dynamic CNR, N-limited photosynthesis, and N-impacted respiration rate every 3 hours. C loss and potential N uptake accumulate within one day in the C-N interface framework, and plant C and N litterfall are transferred to DayCent-SOM at the end of the day. DayCent-SOM calculates the amount of inorganic N available for plant N uptake (N_{avail}) and the N losses from nitrate leaching and N-trace gas emissions each day. The TRIFFID updates the vegetation dynamics based on the C balance on day 10, including PFT competition. The updated vegetation dynamics are transferred to SSiB5 to calculate N-limited phenology to reflect the impact of N on the C cycle, which is significant during the growth season.

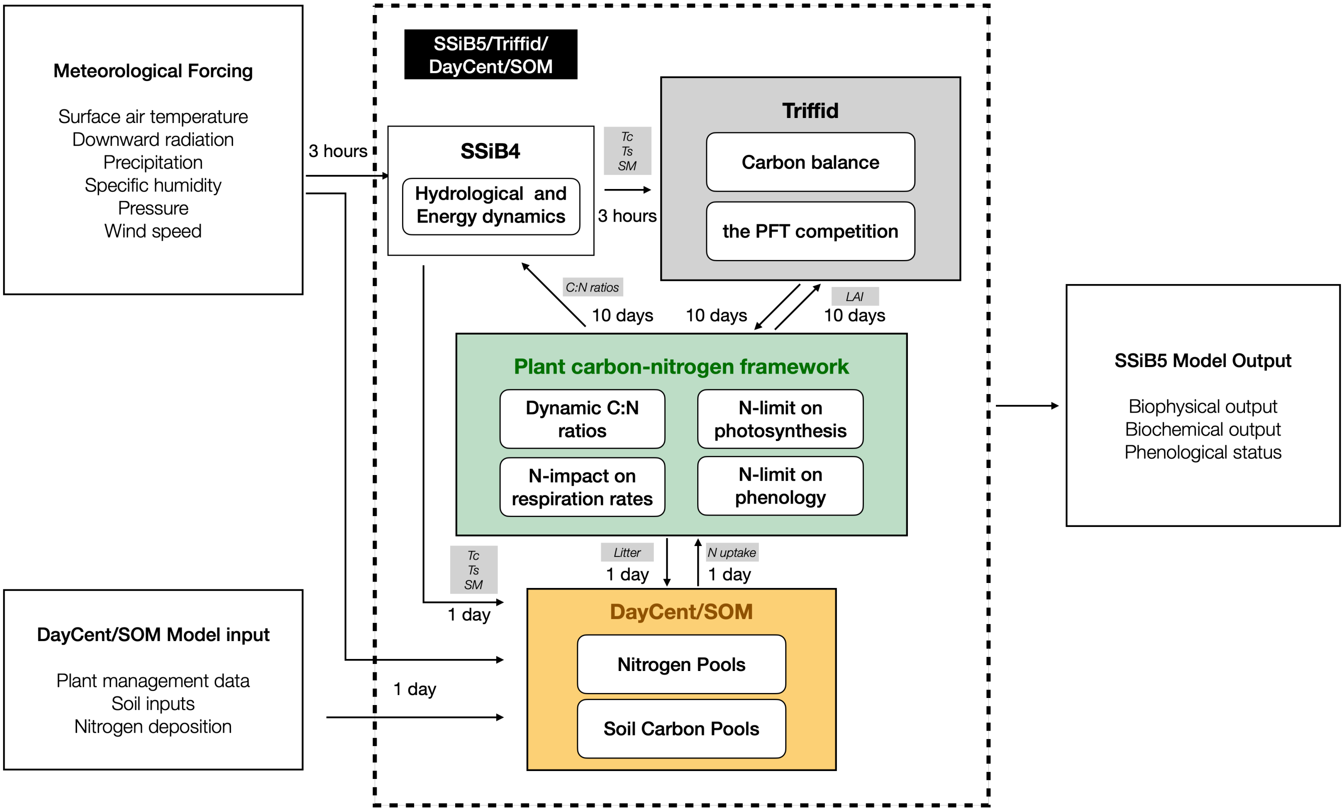

Figure 3. Flowchart of plant carbon-nitrogen interactions in SSiB5/TRIFFID/DayCent-SOM; the main variables between the two modules are listed.

Notes: Tc: canopy temperature; Ts: land surface temperature; SM: soil moisture; GPP: gross primary productivity; Res: autotrophic respiration.

2.3 Model forcing and validation data

Long-term measurements from flux tower sites with different PFTs and global satellite-derived products are employed as references to systematically assess the effects of this coupling framework and N limitation on the terrestrial carbon cycle. Flux tower site data are presented in section 2.3.1. The global meteorological forcing and validation data are listed in sections 2.3.2 and 2.3.3, respectively.

2.3.1 Ground measurement data

To validate the coupled model, thirteen sites with representative biome types and climate zones were selected to evaluate the simulations of the seasonal patterns of GPP, sensible heat flux, and latent heat flux. All driving data were a half-hourly dataset, including air temperature, specific humidity, wind velocity, air pressure, precipitation, and shortwave and longwave radiation data from the FLUXNET 2015 dataset (Pastorello et al., 2020). The GL-ZaH data were obtained from a tundra heath site (Lund et al., 2012). The geographical distribution of the selected FLUXNET 2015 sites is displayed in Figure 4, and the detailed site information is listed in Table 4.

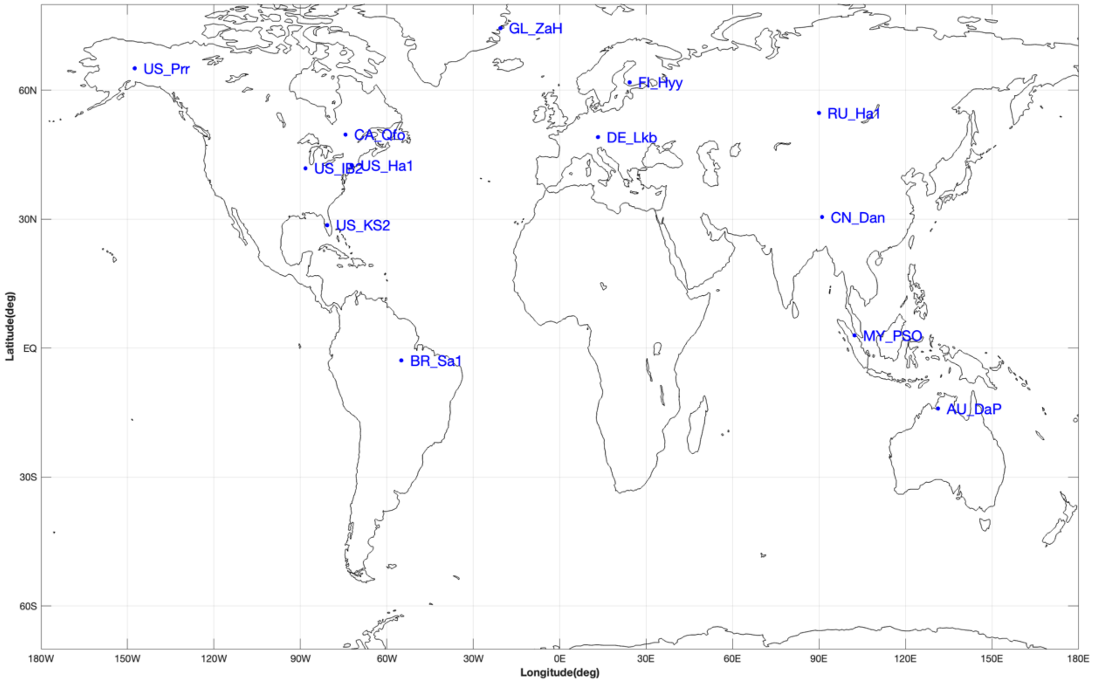

Figure 4. Geographical distribution of selected FLUXNET 2015 sites. The information on these FLUXNET sites is listed in Table 4.

Table 4. The FLUXNET sites, latitude (LAT), longitude (LONG), plant function type (PFT), and time frame (Time) used for the SSiB5/TRIFFID/DayCent-SOM model validation.

Site_ID	Site name	LAT	LONG	PFT	Time
AU_DaP	Daly River Savanna	-14.06	131.32	C4 plants	2007-2013
BR-Sa1	Santarem-Km67-Primary Forest	-2.86	-54.96	Broadleaf Evergreen	2002-2011
CA_Qfo	Quebec - Eastern Boreal, Mature Black Spruce	49.69	-74.34	Needleleaf Evergreen	2003-2010
CN-Dan	Dangxiong	30.50	91.07	C3 grass	2004-2005
DE_Lkb	Lackenberg	49.10	13.30	Needleleaf Evergreen	2009-2013
FI_Hyy	Hyytiala	61.85	24.29	Needleleaf Evergreen	1996-2014
MY_PSO	Pasoh Forest Reserve	2.97	102.31	Broadleaf Evergreen	2003-2009
RU_Ha1	Hakasia steppe	54.73	90.00	C3 grass	2002-2004
US_Ha1	Harvard Forest EMS Tower (HFR1)	42.54	-72.17	Broadleaf deciduous	1991-2012
US_IB2	Fermi National Accelerator Laboratory- Batavia (Prairie site)	41.84	-88.24	C3 grass	2004-2011
US-KS2	Kennedy Space Center (scrub oak)	28.61	-80.67	Shrub	2003-2006
US_Prr	Poker Flat Research Range Black Spruce Forest	65.12	-147.49	Needleleaf Evergreen	2010-2014
GL_ZaH	Zackenberg Heath	74.47	-20.55	Tundra	2000-2014

2.3.2 Meteorological forcing data

The Princeton global meteorological dataset for land surface modeling (Sheffield et al., 2006) was used to drive the SSiB4/TRIFFID global simulations from 1948 to 2007 at 1° x 1° spatial resolution and a 3-hour temporal interval. This dataset, which included surface air temperature, pressure, specific humidity, wind speed, downward shortwave radiation flux, downward longwave radiation flux, and precipitation, was constructed by combining a suite of global observation-based datasets with the National Center for Environmental Prediction/National Center for Atmospheric Research reanalysis data.

2.3.3 Global remote-sensing data

To assess the climatological status, variation, and trends of the simulated LAI, two widely used global LAI products were used as references in this study: the Global Inventory Modeling and Mapping Studies (GIMMS) LAI and the Global LAnd Surface Satellite (GLASS) LAI. GIMMS-LAI is based on the third generation of the normalized difference vegetation index (NDVI3g) from the GIMMS group and an artificial neural network model (Zhu et al., 2013). GIMMS-LAI provides a 1/12-degree resolution, 15-day composites, and spans from July 1981 to December 2011. GLASS-LAI is generated from Advanced Very

High Resolution Radiometer (AVHRR) (from 1982 to 1999 with 0.05-degree resolution) and Moderate Resolution Imaging Spectroradiometer (MODIS, from 2000 to 2012 with 1 km resolution) reflectance data using general regression neural networks (Xiao et al., 2014). The GIMMS and GLASS LAIs and the meteorological forcing data for the overlap period from 1982 to 2007 were remapped to a 1-degree spatial resolution and a monthly temporal interval.

The Model Tree Ensemble (MTE) GPP product (Jung et al., 2009) was used as a reference to evaluate the simulated GPP. MTE is based on a machine learning technique in which the model is trained to predict the five C fluxes at FLUXNET sites driven by observed meteorological data, land cover data, and the remotely sensed fraction of absorbed photosynthetically active radiation (Jung et al., 2009). The trained model was then applied at the grid scale driven by gridded forcing data. The MTE-GPP data were resampled to a 1-degree spatial resolution and a monthly temporal resolution. However, the MTE data do not include CO_2 fertilization. Liu et al. (2019) discussed this issue and indicated that the lack of CO_2 fertilization mainly affects the trend. Since this paper focuses on climatological means as well as differences between different experiments in which the CO_2 fertilization effect is largely cancelled, the lack of CO_2 fertilization in FLUXNET-MTE is not a factor in interpreting our results.

3 Experimental designs

To illustrate the reliability of the schemes that represent different processes of plant N in our framework, we first evaluated the model's short-term performance using in situ measurements (section 3.2). Then, four sets of sensitivity experiments were designed to quantify the major effects of the plant N process and the relative contributions of different plant N processes on the terrestrial ecosystem carbon cycle (section 3.3).

3.1 Initial conditions for the dynamic vegetation model

The initial condition of the dynamic vegetation SSiB4/TRIFFID needs to be obtained from a long-term equilibrium simulation (Zhang et al., 2015). There are different ways to initialize the surface conditions for quasi equilibrium simulations. Following previous SSiB4/TRIFFID studies (Huang et al., 2020; Liu et al., 2019; Zhang et al., 2015), we set up the initial conditions for the run using the SSiB vegetation map and SSiB vegetation table, which are based on ground surveys and satellite-derived information (Dorman and Sellers, 1989; Sellers et al., 1986; Xue et al., 2004; Zhang et al., 2015) with 100% occupation at each grid point for the dominant PFT and zero occupation for other PFTs. We then ran the SSiB4/TRIFFID model with climate forcing and the atmospheric CO_2 concentration at the 1948 level for 100 years to reach equilibrium. The vegetation and soil conditions from the equilibrium results were used as the initial conditions for the subsequent model runs.

Determining the initial conditions for SSiB5/TRIFFIID/DayCent-SOM was carried out as described for SSiB4/TRIFFID with one additional step to initialize the global soil C and N levels. We saved 60 years of daily litter C/N inputs and soil temperature and moisture conditions from the SSiB4/TRIFFID, which were based on historical meteorological forcings (1948-2007). An offline version of DayCent-SOM was run for 2000 years for each grid cell using these 60 years of data, repeated repeatedly, to determine the quasi-equilibrium soil C and N levels; these soil C and N values were read in by SSiB5/TRIFFIID/DayCent-SOM at the start of the global simulation in 1948. This approach was applied for both measurement sites and global 2-D simulations.

3.2 Site-level validation

This paper focuses on the impact of N processes on the climatology of the global carbon cycle. Most current dynamic global vegetation models (DGVMs) are mainly focused on long-term (decadal to thousands of years or even longer) simulations at the global scale; diurnal and seasonal variations are not the subject of their modeling. Moreover, adequate long-term in situ measurements are not available for comparison. However, since the SSiB5/TRIFFID is a process-based model, we can evaluate the model's short-term performance using in situ measurements.

Thirteen sites with representative biome types and climate zones (Table 4 and Fig. 4) were selected to evaluate the simulations of seasonal patterns of fluxes across these sites. Site-level simulations were conducted by SSiB4/TRIFFID (a C-only model) and SSiB5/TRIFFID/DayCent-SOM separately to validate the model's performance. The model results were compared against the observed daily data obtained by the flux tower, including the GPP, sensible heat flux, and latent heat flux.

3.3 Global 2D offline control runs and sensitivity runs

In this study, SSiB4/TRIFFID and SSiB5/TRIFFID/DayCent-SOM were applied to conduct a series of global 2D offline runs (Table 5). All these runs employed the quasi-equilibrium simulation results as the initial conditions and were then driven by the historical meteorological forcing from 1948 through 2007. The run using SSiB4/TRIFFID is referred to as the control run (Exp. SSiB4 hereafter). Using the control simulation, we first evaluated the ability of the model to produce the climatology and variability of several biotic variables by comparing the results to multiple observation-based datasets. In addition to the control run, four sets of sensitivity experiments were conducted to quantify the major effects of the N process and C–N interface coupling methodology on the C cycle. These sensitivity experiments were designed as follows:

(1) Nitrogen limitation on photosynthesis (Exp. NlPSN): The same meteorological forcing used for the control (Exp. SSiB4) drives the model, but dynamic CNR and N limitation on $V_{c,max}$ (Eq. 6) are introduced. The difference between Exp. SSiB4 and Exp. NlPSN indicates the effect of N limitation on photosynthesis.

(2) Nitrogen impact on respiration rate (Exp. NlResp): The model was driven by the same meteorological forcing used for Exp. SSiB4, but dynamic CNR and N impacts on autotrophic respiration (Eq. 10) are introduced. The difference between Exp. SSiB4 and Exp. NlResp indicates the effect of N on the respiration rate.

(3) Nitrogen limitation on Phenology (Exp. NlPhen): The model was driven by the same meteorological forcing used for Exp. SSiB4, but dynamic CNR and N impacts on phenology (Eq. 13) were introduced. The difference between Exp. SSiB4 and Exp. NlPhen indicates the effect of nitrogen limitation on phenology.

(4) SSiB5/TRIFFID/DayCent-SOM (Exp. SSiB5): The model was driven by the same meteorological forcing used for Exp. SSiB4, but all four C-N coupling processes in the framework, i.e., dynamic CNR, N impacts on photosynthesis, autotrophic

respiration, and phenology, are introduced. The difference between Exp. SSiB4 and Exp. SSiB5 indicates the effect of N dynamics, especially the sensitivity of C cycle variability and trends to N process coupling. Furthermore, the difference between Exp. NlPSN and Exp. SSiB5 indicates uncertainty (or possible errors) due to missing N effects on autotrophic respiration and phenology in the coupling framework.

Although the model runs were from 1948 to 2007, we only present the results from 1982-2007 to avoid spinning up for the SSiB5/TRIFFID/DayCent-SOM after SSiB4/TRIFFID and DayCent-SOM each reached their historical equilibrium conditions. Since the results from Exps. SSiB5 and NlPSN showed statistically significant differences from Exp. SSiB4 over many parts of the world; in the following discussion, we will mainly focus on the differences between these two experiments and Exp. SSiB4.

Table 5. Experimental design

100-year equilibrium → ***Initial condition***	Real-forcing simulation 1948-2007	
Fixed climatology forcing	*Transient forcing*	
Control experiment	**SSiB4:**	Control experiment
	NlPSN:	**N**itrogen **l**imitation on **p**hoto**syn**thesis (Vmax), Eq.6
	NlResp:	Nitrogen impact on Respiration rate, Eq.10
	NlPhen:	Nitrogen limitation on Phenology, Eq. 13
	SSiB5:	including all four nitrogen processes

4. Results

To test this framework, measurements from flux tower sites with different PFTs and global satellite-derived products from 1982–2007 are employed as references. The results from site simulation and global 2-D simulations are presented in sections 4.1 and 4.2, respectively. As mentioned in section 2, the framework takes some plant N metabolism processes into account. To illustrate the relative contributions of different plant N processes to the terrestrial ecosystem carbon cycle, four sets of sensitivity experiments were designed (Table 5). The analyses are presented in section 4.2.

4.1 Evaluations using measurements from flux tower sites

Land models with dynamic vegetation and nitrogen processes normally focus on long-term climate simulations at large spatial scales. In this section, we validate the model performance for thirteen sites with several years of simulation (Table 4) to ensure that, as a process-based model, the short-term SSiB5/TRIFFID simulation is still able to properly represent the surface processes at seasonal scales after the introduction of DayCent-SOM through the interface coupling framework. This evaluation also provides a glance at the model's performance at several sites with various climates and PFTs (Table 4) with short-term data to gain preliminary confidence for further evaluation.

Figures 5, 6, and 7 show that both SSiB4 and SSiB5/TRIFFID/DayCent-SOM produce a reasonable seasonal cycle for GPP, sensible heat, and latent heat fluxes, respectively, and that the results are close to the observations. Table 6 summarizes the major results. We use bias, root-mean-square error (RMSE), and standard deviation to assess model performance against in situ site measurements. When we evaluated the average of the 13 sites, the biases for GPP and sensible and latent heat fluxes decreased by approximately 7%, 17%, and 2%, respectively. The average RMSEs over the 13 sites for these three variables also decreased by approximately 2%, consistent with the reduction in bias. Furthermore, SSiB5/TRIFFID/DayCent-SOM produced a closer standard deviation for GPP, sensible heat flux, and latent heat flux than did SSiB4/TRIFFID for the 13-site averages. Overall, in these short-term simulations with specified initial vegetation conditions, both SSiB4 and SSiB5 produce reasonable GPP and surface heat fluxes compared with in situ measurements, but adding N processes (SSiB5) slightly improved the 13-site average. Although these improvements are rather marginal (except for the bias reduction for sensible heat), the results nevertheless demonstrate that, with short-term simulation, the improvement in the model simulations is rather consistent.

With closer checking of the SSiB4 to SSiB5 results at each site, the results display various characteristics. For instance, while some sites showed improvements in all three variables (GPP and latent and sensible heat fluxes), others only showed improvements in one or two variables. It should be noted that SSiB4 and SSiB5 are mainly used for global studies. For the validation of in situ measurements, proper optimization of some site-specific soil and vegetation parameters is necessary (Xue et al., 1996, 1997). In this study, no model parameters were optimized during this validation exercise for a better fit between the simulated results and FLUXNET measurements. The discussions above led us to conduct long-term experiments at a global scale to comprehensively investigate the effects of N processes and to help understand the mechanisms governing the global carbon cycle, which will be discussed in the following section.

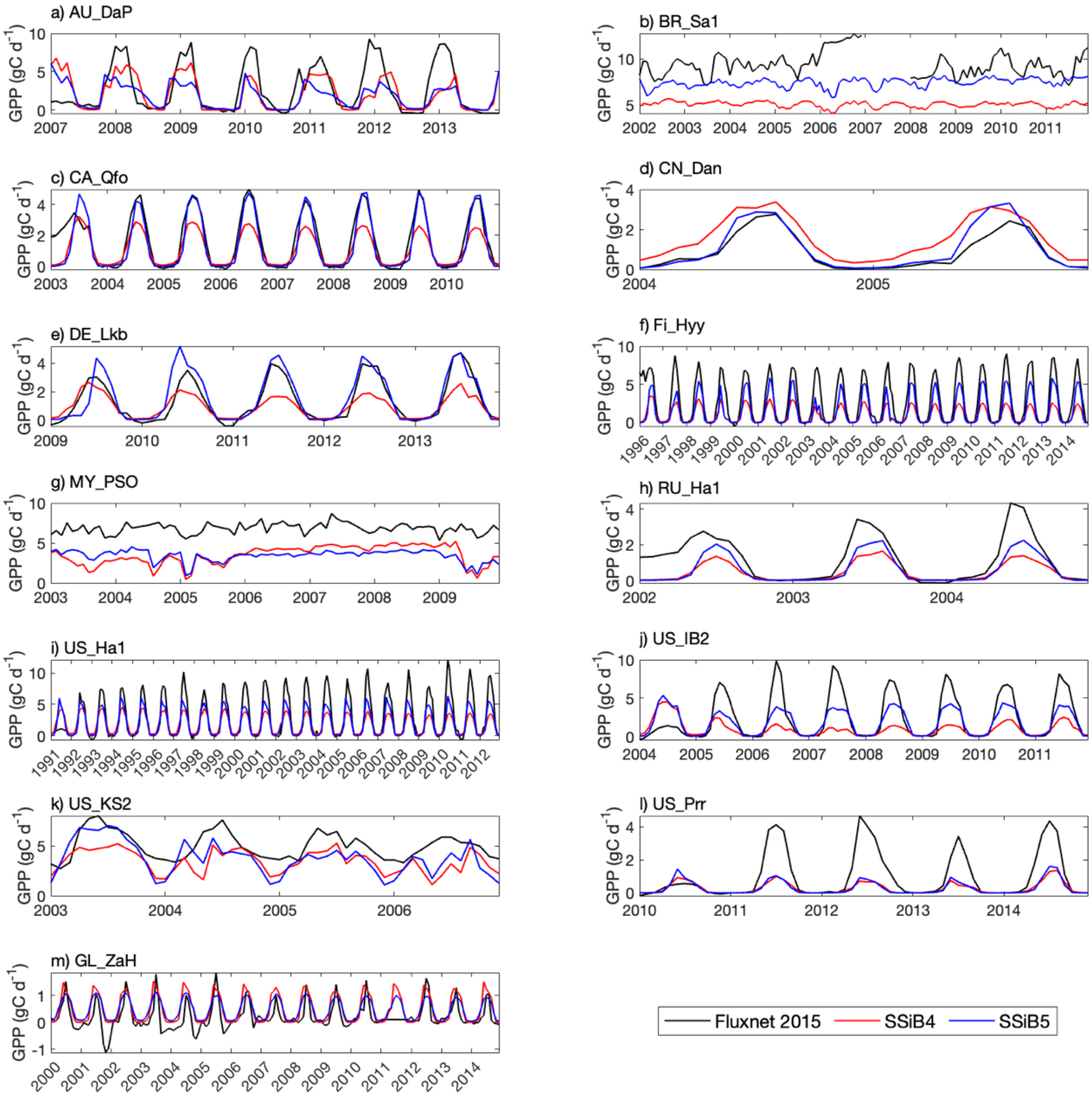

Figure 5. Simulated seasonal variations in GPP against observations at thirteen sites representing different SSiB5 PFTs.

Note: The information about these FLUXNET sites is listed in Table 4.

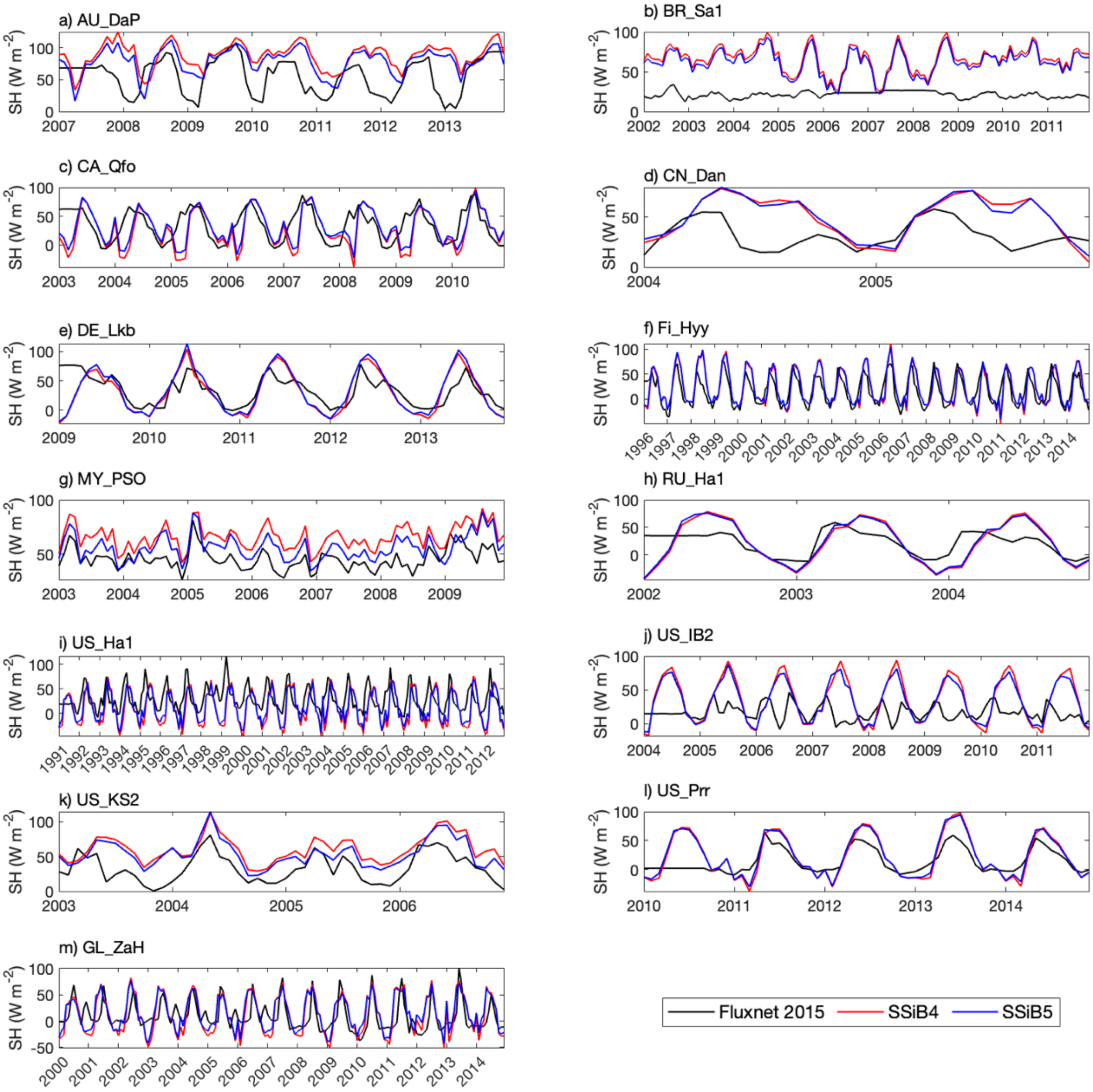

Figure 6. Same as Figure 5 but for sensible heat flux.

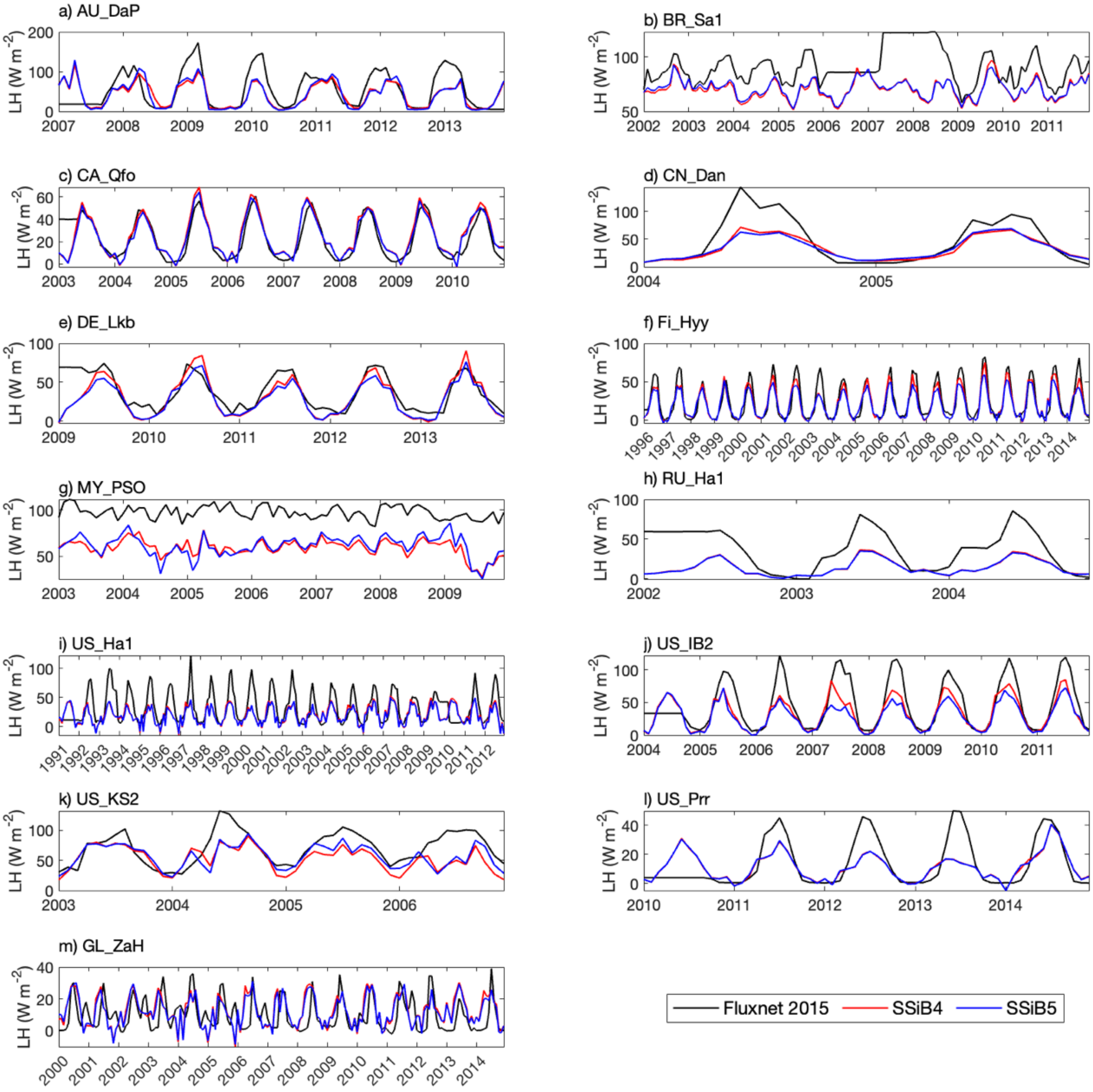

Figure 7. Same as Figure 5 but for the latent heat flux.

Table 6. The GPP, sensible heat flux, and latent heat flux comparisons of bias, standard deviation and RMSE between SSiB4 and SSiB5 at the thirteen sites.

	Site_ID	Bias		Standard deviation			RMSE	
		SSiB4	SSiB5	Fluxnet	SSiB4	SSiB5	SSiB4	SSiB5
GPP (g C d^{-1})	AU_DaP	0.05	-0.05	3.11	2.46	2.33	2.60	2.61
	BR-Sa1	-1.07	-1.20	1.31	0.57	0.55	1.77	1.84
	CA_Qfo	-0.05	-0.11	1.71	1.99	1.92	0.78	0.75
	CN-Dan	0.70	0.08	0.92	1.08	1.03	0.80	0.33
	DE_Lkb	0.34	0.25	1.50	1.80	1.71	0.80	0.74
	FI_Hyy	-0.11	-0.22	2.93	3.47	3.32	1.51	1.44
	MY_PSO	-1.02	-1.20	0.65	1.28	1.21	1.63	1.72
	RU_Ha1	-0.24	-0.27	1.29	1.31	1.27	0.69	0.69
	US_Ha1	0.36	0.27	3.31	3.36	3.30	1.31	1.28
	US_IB2	0.56	0.42	2.91	2.70	2.57	1.80	1.79
	US-KS2	-0.28	-0.52	1.37	1.76	2.01	1.35	1.54
	US_Prr	-0.08	-0.10	1.43	1.30	1.28	0.86	0.86
	GL_ZaH	0.28	0.25	0.50	0.53	0.37	0.48	0.43
13-site average		**0.40**	**0.37**	**1.76**	**1.82**	**1.76**	**1.26**	**1.23**
Sensible Heat Flux (W m^{-2})	AU_DaP	32.47	23.13	28.26	19.64	21.05	36.24	36.32
	BR-Sa1	45.29	40.94	4.04	16.32	15.98	25.61	25.07
	CA_Qfo	-7.04	-2.34	27.77	33.18	29.37	9.54	9.20
	CN-Dan	17.96	18.53	14.44	22.38	20.75	25.60	26.99
	DE_Lkb	-3.12	0.16	25.13	35.39	36.91	17.83	18.15
	FI_Hyy	5.53	7.20	28.17	33.57	33.63	8.99	10.91
	MY_PSO	20.49	10.86	10.03	11.30	11.98	39.22	37.99
	RU_Ha1	-0.14	0.84	21.71	39.19	38.02	29.42	29.67
	US_Ha1	-18.34	-15.80	24.40	33.71	29.42	24.33	24.66
	US_IB2	20.21	18.26	11.95	32.89	29.19	23.16	28.72
	US-KS2	27.74	20.81	21.01	19.17	20.14	27.31	24.73
	US_Prr	8.10	9.35	20.93	36.84	35.45	12.02	12.01
	GL_ZaH	2.24	5.03	27.08	36.04	31.48	29.20	27.37
13-site average		**16.05**	**13.33**	**20.38**	**28.43**	**27.18**	**23.73**	**23.98**
Latent Heat Flux (W m^{-2})	AU_DaP	-11.02	-10.83	45.72	30.03	33.93	36.24	36.32
	BR-Sa1	-20.47	-19.82	16.15	9.44	8.47	25.61	25.07
	CA_Qfo	2.21	0.96	18.06	18.63	17.56	9.54	9.20
	CN-Dan	-12.63	-12.57	42.39	22.13	20.77	25.60	26.99
	DE_Lkb	-7.39	-10.00	22.81	24.57	20.79	17.83	18.15
	FI_Hyy	-3.06	-4.84	23.22	19.21	16.64	8.99	10.91
	MY_PSO	-38.18	-36.18	7.07	9.24	11.64	39.22	37.99
	RU_Ha1	-22.89	-23.10	25.68	10.43	10.08	29.42	29.67
	US_Ha1	-11.94	-13.14	27.06	15.53	14.71	24.33	24.66
	US_IB2	-12.90	-17.38	36.91	24.68	20.70	23.16	28.72
	US-KS2	-17.74	-13.41	27.63	20.28	19.65	27.31	24.73
	US_Prr	-1.90	-1.87	16.44	9.62	9.68	12.02	12.01
	GL_ZaH	2.76	2.26	10.17	9.67	9.17	11.15	10.48
13-site average		**12.80**	**12.70**	**24.56**	**17.19**	**16.45**	**22.68**	**22.34**

4.2 Evaluation of GPP and LAI at the Global Scale

The SSiB model is mainly used for global climate studies. It is important to adequately produce the observed global GPP and LAI. The model's performance in these aspects is evaluated in this section. The SSiB4/TRIFFID-simulated global PFT distribution has been extensively discussed in Zhang et al. (2015) and Liu et al. (2019). The simulation results are generally consistent with observation. The spatial distribution from the SSiB5/TRIFFID/DayCent-SOM did not show substantial difference and will not be discussed here. The simulated GPP averaged over 1982-2007 was compared to the FLUXNET-MTE GPP (Jung et al., 2011) to examine the impact of N processes and their coupling with C and ecosystem processes. Both SSiB4/TRIFFID (Exp. SSiB4) and SSiB5/TRIFFID/DayCent-SOM (Exp. SSiB5) capture the distribution of global GPP (Fig. 8) and its latitudinal distribution (Fig. 9a).

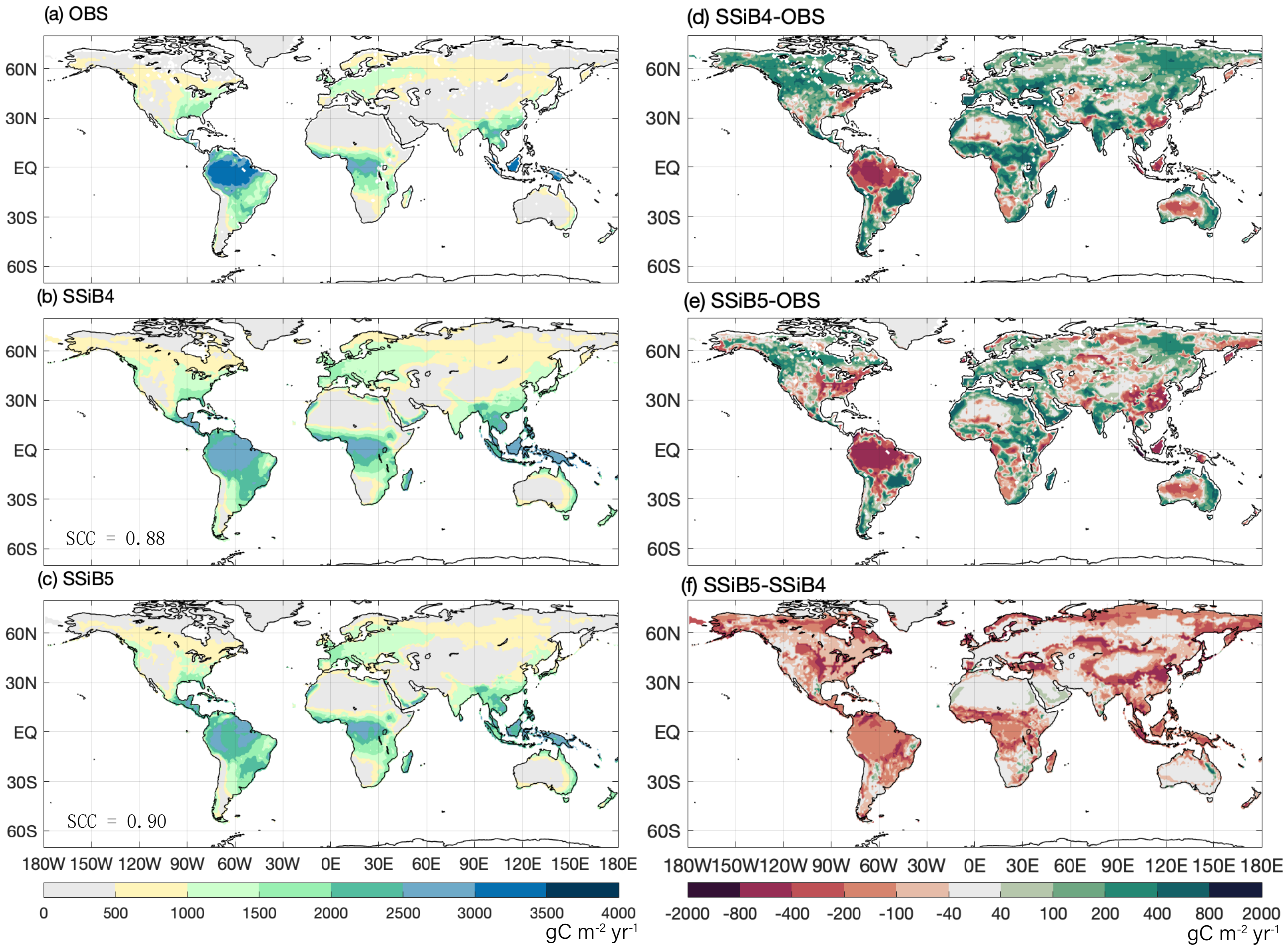

Figure 8. The 1982-2007 average gross primary production comparison for (a) FLUXNET-MTE GPP (OBS), (b) SSiB4/TRIFFID (SSiB4), and (c) SSiB5/TRIFFID/DayCent/SOM (SSiB5) and the difference between (d) SSiB4-OBS, (e) SSiB5-OBS, and (f) SSiB5-SSiB4. Note: SCC indicates the spatial correlation coefficient between the model simulation and satellite-derived datasets (OBS).

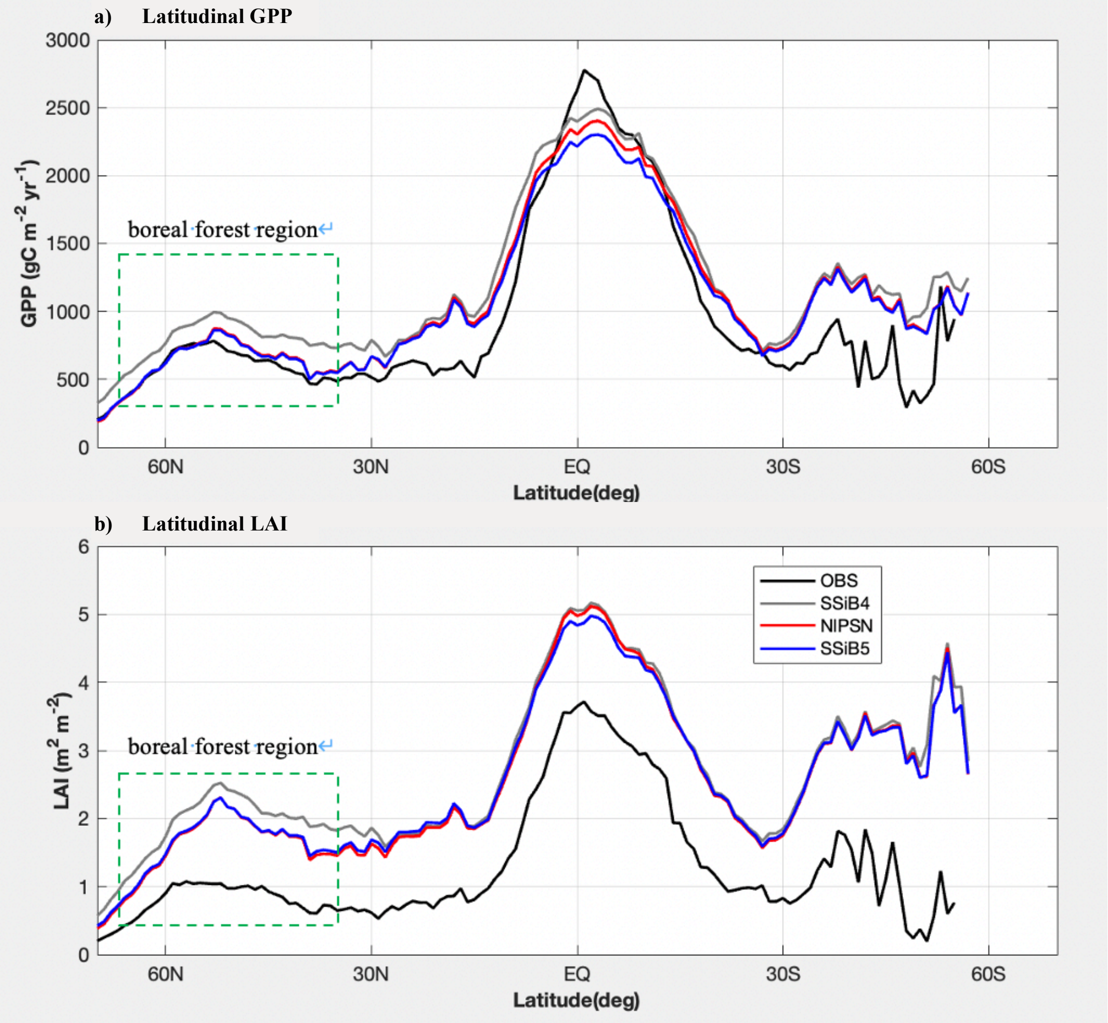

Figure 9. Intercomparisons of latitudinal LAI and GPP among OBS, SSiB4 (control), NlPSN (N limitation on photosynthesis only), and SSiB5 (all N processes) over the period of 1982-2007.

Note: Observed LAI is the GIMMS LAI.

510

Table 7. Regional and global GPP for (a) FLUXNET-MTE GPP (observation), (b) SSiB4 (control), (c) NlPSN (N limitation on photosynthesis only) and (d) SSiB5 (N limitation on photosynthesis, autotrophic respiration, and phenology).

Regions	Sub-regions	GPP Mean (gC m^{-2} yr^{-1})							
		MTE		**SSiB4**		**NlPSN**		**SSiB5**	
		mean	**bias**	**mean**	**bias**	**mean**	**bias**	**mean**	**bias**
Arid and Semi-Arid Areas	West Africa	893		1147	254(28.5%)	963	70(7.9%)	915	22(2.5%)
	West NA	438		549	111(25.4%)	454	16(3.5%)	431	-7(-1.6%)
	SA Savanna	1665		1860	195(11.7%)	1763	98(5.9%)	1675	10(0.6%)
	East Africa	1228		1533	306(24.9%)	1427	199(16.2%)	1356	128(10.4%)
	East Asian semi-arid	1440		1470	30(2.1%)	1199	-241(-16.7%)	1139	-301(-20.9%)
NH High-Mid Latitude Areas	NA High-Mid Latitude	552		814	262(47.6%)	700	149(27.0%)	665	114(20.6%)
	Eurasian High-Mid	844		966	122(14.5%)	871	27(3.2%)	827	16(-2.0%)
Equator	Amazon Basin	2993		2668	-326(-10.9%)	2631	-362(-12.1%)	2500	-494(-16.5%)
	Southeast Asia	2778		2540	-238(-8.6%)	2419	-359(-12.9%)	2298	-480(-17.3%)
	Equator Africa	2522		2645	123(4.9%)	2611	89(3.5%)	2481	-42(-1.7%)
Subarctic Areas and Tibet	NA Subarctic	234		364	130(55.7%)	240	6(2.4%)	228	-6(-2.7%)
	Eurasian Subarctic	331		484	153(46.2%)	328	-3(-1.0%)	311	-20(-6.0%)
	Tibet	409		561	153(37.3%)	298	-111(-27.2%)	283	126(-30.8%)
Global		**863**		**1082**	**220(25.4%)**	**991**	**129(14.9%)**	**942**	**79(9.1%)**

Note: the numbers in parentheses are relative biases: (bias/MTE mean)

The highest GPP occurs in tropical evergreen forests and generally decreases with increasing latitude according to both the observations and the model simulations (Figs. 8 and 9a). Exp. SSiB4-simulated GPP has a positive bias over many parts of the world (Fig. 8d), including tropical Africa and the North American and eastern Siberian boreal regions, but a negative bias in some regions, mainly in the Amazon tropical forest. The simulated global GPP is 1082.36 g C m^{-2} yr^{-1} (Table 7), which is higher than the estimated value of 862.86 g C m^{-2} yr^{-1} in FLUXNET-MTE (Jung et al., 2011). After introducing N limitation for the three processes, SSiB5 reduced the positive bias in SSiB4 over many parts of the world (Figs. 8e, 8f, and 9a). Exp. SSiB5's global GPP prediction, 941.81 g C m^{-2} yr^{-1}, is closer to the observations than Exp. SSiB4, with a 16.3% reduction in the bias (Table 7). Furthermore, the temporal correlation coefficients between the observed and simulated monthly/annual mean GPPs increased from 0.46/0.98 (Exp. SSiB4) to 0.50/0.99 (Exp. SSiB5), respectively (Fig. 10), showing improvement in the simulation of the seasonal cycle in SSiB5. The correlation for interannual variability in SSiB4 is already very high (0.98). SSiB5 continues the high correlation of SSiB4.

The improvement, however, is not homogeneous across the globe but displays apparent regional characteristics. The GPP biases in tropical Africa, the North American boreal region, the South American savanna, and the central U.S. showed substantial reductions (Fig. 8f), which helped improve the spatial distribution of SSiB5. The global spatial correlation coefficient increases from 0.88 to 0.90 (Fig. 8). Moreover, the GPP simulations did not improve in some regions, such as in temperate East Asian mixed forest-grassland regions and in some areas of Siberia (Fig. 8). In particular, the negative GPP bias in the Amazon increased (Fig. 8f). This phenomenon also appeared in the offline test at the Amazon site (the BR-Sa1 site, Table 4). Du et al. (2020) indicated that phosphorus (P) has a greater effect in tropical areas.

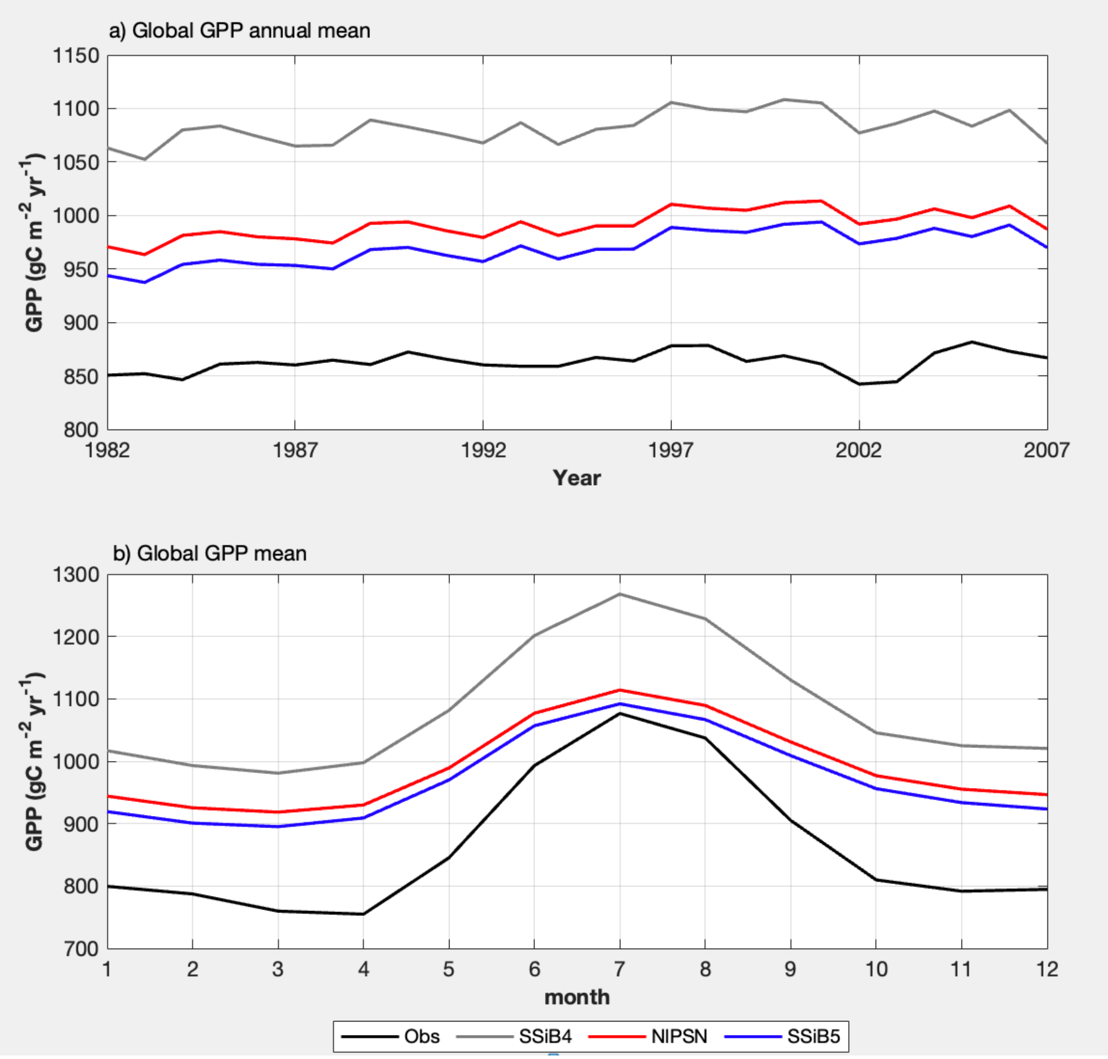

535 **Figure 10.** Intercomparisons of global monthly/annual mean GPPs among OBS, SSiB4 (control), NlPSN (N limitation on photosynthesis only), and SSiB5 (all N processes) over the period of 1982-2007.

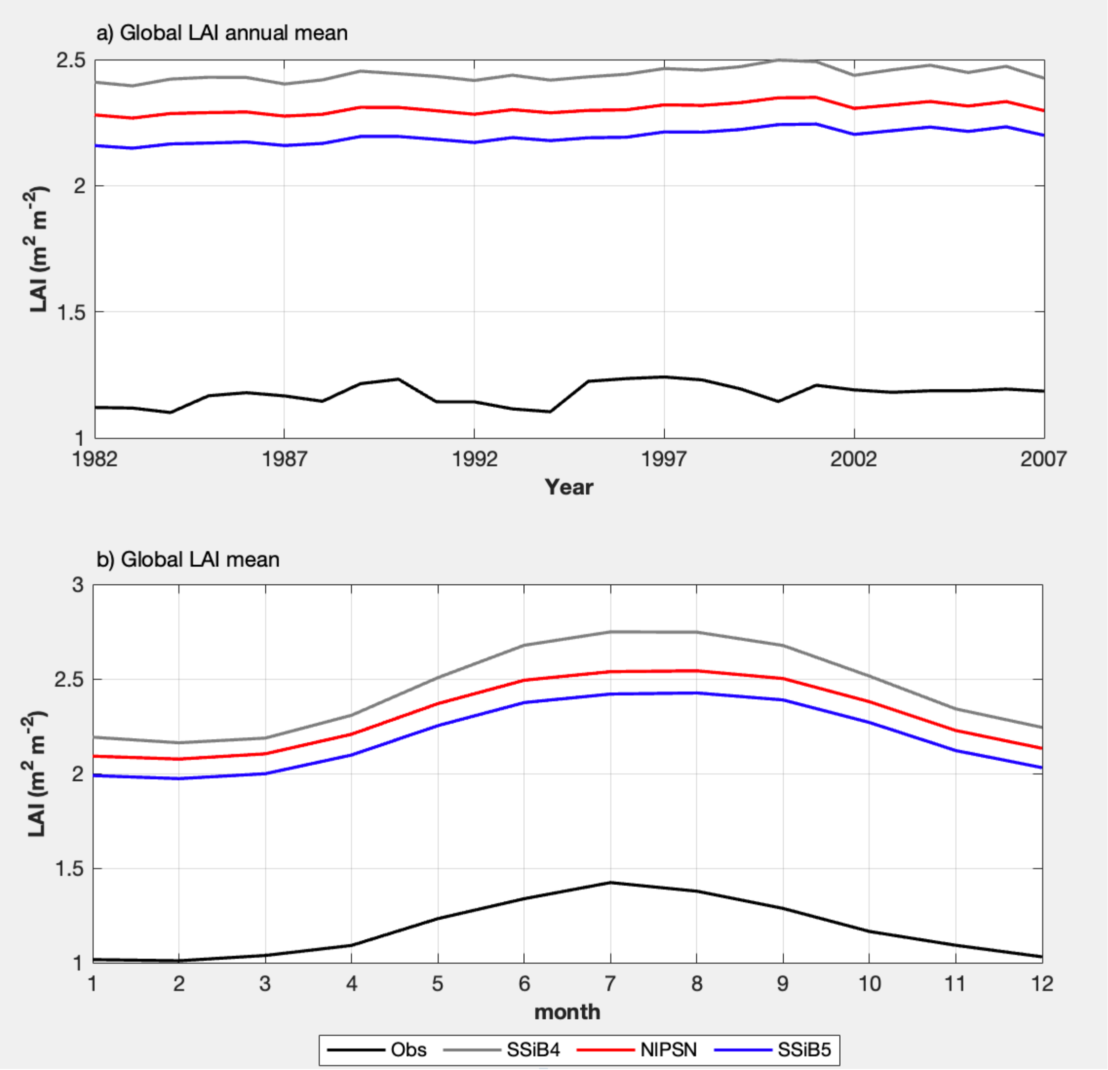

Figure 11. Same as Figure 10 but for the LAI.

Note: Observed LAI is the GIMMS LAI.

Furthermore, the effect of N limitations on the LAI simulation was also investigated. Compared with satellite-derived products, both SSiB4 and SSiB5 exhibit reasonable spatial distributions (Figs. 12a-c). The highest LAI occurs in tropical evergreen forests and decreases with latitude in both the observations and the model (Fig. 9b). Compared with the control, Exp. SSiB5 also generally reduced the positive bias in the simulated LAI (Fig. 12f). The simulated LAI in Exp. SSiB4 has a global positive bias. After introducing the three N limitation processes, the positive bias decreased over most parts of the world (Fig. 12f). Globally, Exp. SSiB5 has an LAI bias of 0.94/1.12 for GIMMS/GLASS, respectively (Table 8), which is lower than the LAI bias of 1.26/1.44 for GIMMS/GLASS, respectively, in Exp. SSiB4, with a substantial 31.1% reduction in the bias (compared to GIMMS, Table 8). However, a substantial positive bias still exists across the globe (Fig. 12e). Our study showed that imposing N limitation is an adequate step to overcome dynamic vegetation models' systematic LAI positive bias, but this issue has still not been resolved and requires further investigation. In addition, the correlation coefficients between the observed and simulated monthly/annual average LAIs improved from 0.49/0.97 (Exp. SSiB4) to 0.51/0.98 (Exp. SsiB5) (Fig. 11).

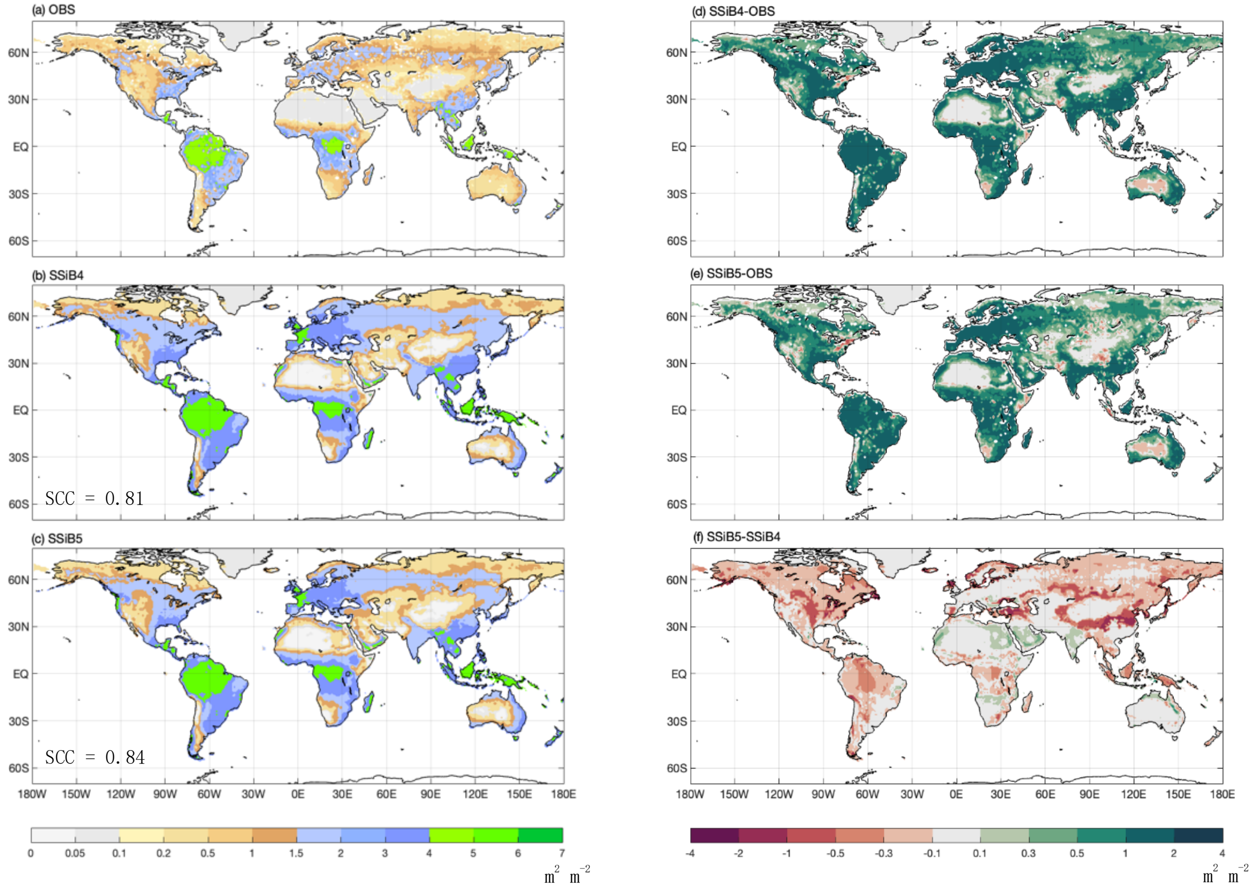

Figure 12. Same as Figure 8 but for the LAI.

Note: SCC indicates the spatial correlation coefficient between the model simulation and the GIMMS LAI (OBS).

It is interesting to note that despite the global general LAI reduction, SSiB5 slightly increased the LAI estimation in North Africa and India (Fig. 12). The impacts of N on phenology and respiration cause a slight shift in vegetation from shrubs (N. Africa) or C4 plants (India) to C3 grasses in these areas, which contributes to the increases in GPP and LAI (Fig. 13). Furthermore, in areas such as the Amazon and East Asian mixed forest-grassland regions, SSiB5 improved only the LAI simulation and not the GPP simulation.

Table 8. Regional and global LAI for (a) GIMMS LAI (observation), (b) GLASS LAI (second observation), (c) SSiB4 (control), (d) NlPSN (N limitation on photosynthesis only) and (d) SSiB5 (N limitation on photosynthesis, autotrophic respiration, and phenology). The bias is relative to the GIMMS LAI.

Regions	Sub-regions	LAI Mean ($m^2 m^{-2}$)									
		GIMMS		GLASS		SSiB4		NlPSN		SSiB5	
		mean	bias	mean	bias	mean	bias	mean	bias	mean	bias
Arid and Semi-Arid Areas	West Africa	1.08		1.01	-0.07(-6.5%)	2.04	0.96(88.9%)	1.89	0.81(75.0%)	1.73	0.65(60.2%)
	West NA	0.62		0.49	-0.13(-21.0%)	1.38	0.76(122.6%)	1.18	0.56(90.3%)	1.09	0.47(75.8%)
	SA Savanna	1.99		1.91	-0.18(-4.0%)	3.34	1.35(67.8%)	3.23	1.24(62.3%)	2.97	0.98(49.2%)
	East Africa	1.59		1.55	-0.04(-2.5%)	3.02	1.43(89.9%)	2.89	1.30(81.8%)	2.66	1.07(67.3%)
	East Asian semi-arid	1.60		1.36	-0.24(-15.0%)	3.35	1.75(109.4%)	2.84	1.24(77.5%)	2.61	1.01(63.1%)
NH High-Mid Latitude Areas	NA High-Mid Latitude	0.84		0.49	-0.35(-41.7%)	1.91	1.07(127.4%)	1.66	0.82(97.6%)	1.53	0.69(82.1%)
	Eurasian High-Mid	1.14		0.57	-0.57(-50.0%)	2.29	1.15(100.9%)	2.08	0.94(82.5%)	1.91	0.77(67.5%)
Equator	Amazon Basin	4.19		4.08	-0.11(-2.6%)	6.01	1.82(43.4%)	5.98	1.79(42.7%)	5.50	1.31(31.3%)
	Southeast Asia	3.93		3.88	-0.05(-1.3%)	4.68	0.75(19.1%)	4.68	0.75(19.1%)	4.31	0.38(9.7%)
	Equator Africa	3.83		3.76	-0.07(-1.8%)	5.74	1.91(49.9%)	5.72	1.89(49.3%)	5.27	1.44(37.6%)
Subarctic Areas and Tibet	NA Subarctic	0.32		0.14	-0.18(-56.3%)	0.71	0.39(121.9%)	0.51	0.19(59.4%)	0.47	0.15(46.9%)
	Eurasian Subarctic	0.33		0.12	-0.21(-63.6%)	0.87	0.54(163.6%)	0.65	0.32(97.0%)	0.60	0.27(81.8%)
	Tibet	0.64		0.54	-0.10(-15.6%)	1.36	0.72(112.5%)	0.81	0.17(26.6%)	0.75	0.11(17.2%)
Global		**1.18**		**1.00**	**-0.18(-15.3%)**	**2.44**	**1.26(110.8%)**	**2.31**	**1.13(95.8%)**	**2.12**	**0.94(79.7%)**

Note: the numbers in parentheses are relative biases

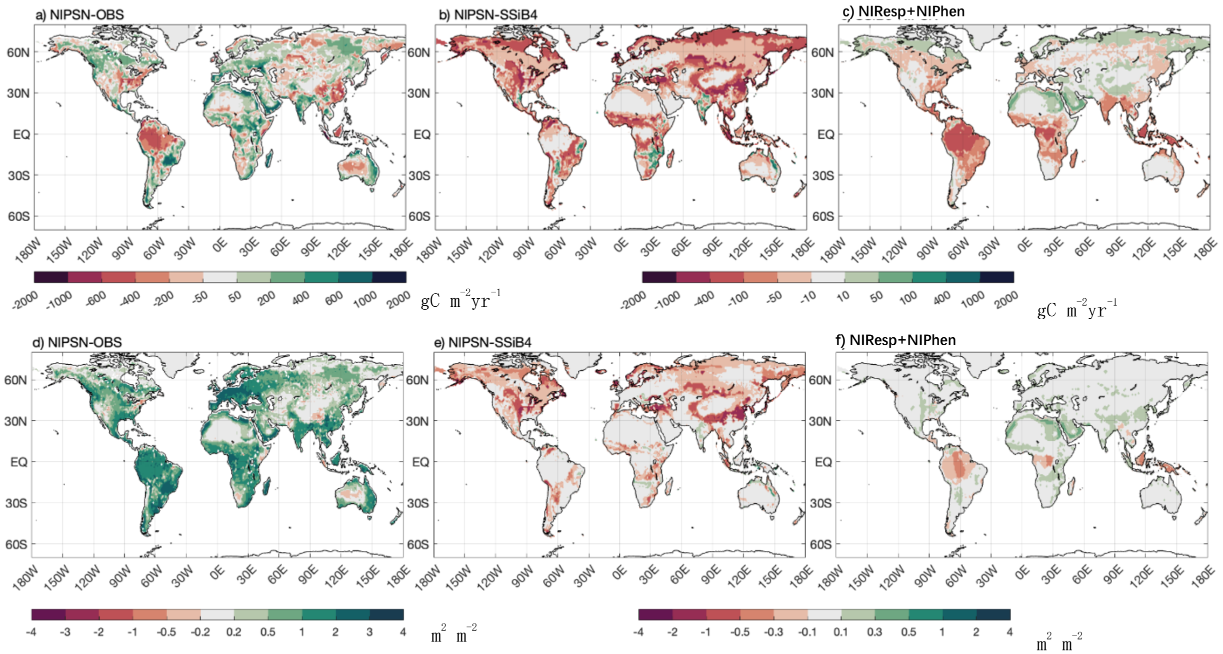

Figure 13. The 1982-2007 average gross primary production difference (a) NlPSN-OBS, (b) NlPSN-SSiB4, (c) NIResp+NIPhen, and leaf area index difference (d) NlPSN- OBS, (e) NlPSN- SSiB4, (f) NIResp+NIPhen

Note: NlPSN is N limitation on photosynthesis (Vc, max) only.

We imposed N limitation on several processes. Among them, Exp. NIPSN has the largest and most significant impact. This paper mainly discusses the results from Exp. NlPSN, which applies Eq. (6) to scale down the $V_{c,max}$.Exp. NIPSN has a lower global GPP bias (128.52 g C m^{-2} yr^{-1}) than does Exp. SSiB4 (219.50 g C m^{-2} yr^{-1}) (Fig. 13, Table 7), but it is larger than that of Exp. SSiB5, in which the bias is 79 g C m^{-2} yr^{-1} (Table 7). In addition, Exp. NlPSN has a global LAI bias of 1.13 (Fig. 13, Table 8), which is also lower than the LAI bias in Exp. SSiB4 (1.26) but higher than that in Exp. SSiB5 (0.94). The largest reductions in the magnitude of the LAI bias are in North America, the Eurasian continent, and tropical savanna regions in South America and Africa (Figs. 13b and 13e). That said, N limitation of photosynthesis plays a dominant role, contributing to approximately 65%/41% of the improvement in the GPP/LAI simulations in Exp. SSiB5, respectively. Adjusting $V_{c,max}$ is the most direct and process-based approach based on physiology and has the greatest impact. However, the effects of N limitation on the other two processes are still substantial. The N limitations on respiration and phenology have the greatest impact in tropical forest and savanna regions (Figs. 13c and 13f). The GPP also reduced the positive bias over boreal regions and the negative bias over polar regions. The results from Exp. NlResp or Exp. NlPhen individually did not show a statistically significant impact. However, the sum of these two N limitations still has substantial impacts on many parts of the world, as displayed in Fig. 13b, mainly in tropical rainforests and some midlatitude regions. In addition, the differences between Exp. SSiB5, which includes three limitations, and Exp. NIPSN, as displayed in Figs. 10 and 11, also delineate the characteristics of the global impacts of these two effects at seasonal and interannual scales.

5 Discussion and Conclusions

This study presents improvements in modeling the C cycle by introducing plant N processes into SSiB5/TRIFFID/DayCent-SOM, using DayCent-SOM to obtain the amount of N available to plants and plant soil N uptake. The approach presented in this study can also be applied to other models with similar physical and biological principles. The new C-N coupling framework allows us to use the dynamic CNR to represent plant resistance and response, which allows adaptations in the stoichiometry of C and N. Since these processes can increase nutrient use efficiency and reduce the impact of N limitation through N remobilization and resorption, the N limitation effect does not linearly or instantaneously respond to the available N content. A linear relationship between the N limitation factor and available N is valid only when N availability is not sufficient for the minimum N demand for new growth. This is an advantage of our approach. With the new model structure, the impacts of N on GPP are predicted directly but not linearly with leaf N content, which is affected by the state of plant growth, autotrophic respiration, and plant phenology.

By comparing site-level results from SSiB4 and SSiB5 to FLUXNET GPP and surface heat fluxes from thirteen sites with representative biome types and climate zones, we gained confidence in the ability of the new N processes to enhance global model performance. We also evaluated the model performance against global satellite product datasets for GPP and LAI. In general, with the new plant C-N coupling framework, SSiB5/TRIFFID/DayCent-SOM produced significantly less absolute bias for GPP and LAI than did the baseline version of SSiB4/TRIFFID (without N processes), with a global decrease in the bias in GPP and LAI of 16.3% and 27.1%, respectively. The main improvements are found in tropical Africa and the boreal forest. The more realistic representation of the dynamic CNR and plant C-N framework leads to general improvements in the global C cycling simulations of SSiB5/TRIFFID/DayCent-SOM. From the perspective of plant physiology (Högberg et al., 2017), the downregulation of the canopy photosynthetic rate based on the available mineral N for the growth of plant tissues is more reasonable than the simple and direct downregulation of GPP or NPP. In fact, we conducted a test to directly downscale GPP and NPP, and our simulation results (not shown) support this viewpoint. This coupled model can better reproduce observed state variables and their emergent properties (such as GPP, NPP, LAI, and respiration).

Despite the general improvement globally, the GPP simulation in temperate East Asian mixed forest-grassland regions seems to be worse with SSiB5 than with SSiB4. In some regions, such as the Amazon, while SSiB4 produced lower GPP than did the observations, the imposed N limitation in SSiB5 further increased the bias in these regions. Recently, the important influence of phosphorus availability on terrestrial ecosystem carbon uptake has been increasingly recognized (Du et al., 2020). Recently, initiated ecosystem-scale manipulation experiments in phosphorus-poor environments (Fleischer et al., 2019) call for the need for new phosphorus-enabled LSMs to track these actions (Goll et al., 2017; Reed et al., 2015). We plan to incorporate other plant processes, such as plant/soil phosphorus processes, to further improve the performance of the model in the future. More evaluations for regions where N limitation is not dominant are necessary.

Although the global GPP of SSiB5 was similar to that of the satellite- derived GPP, the positive bias for the LAI was still very large (Table 7). Recent review papers seem to confirm that overestimation of LAI is a common issue in current dynamic vegetation models. Murray-Tortarolo et al. (2013) and Anav et al. (2013) evaluated the performance of dynamic vegetation models in simulating LAI from a CMIP model intercomparison. The simulated LAI for almost every dynamic vegetation model is twice as large as the satellite-derived LAI. More recent studies (Zaehle et al., 2015; Mueller et al., 2019; Gristina et al., 2020; Oliveira et al., 2021; Heikkinen et al., 2021) have confirmed this shortcoming in current dynamic vegetation models. Further investigations are necessary.

Anthropogenic N input is one of the major factors affecting C–N coupling and N limitation. The anthropogenic N inputs to terrestrial ecosystems have been much greater than the vegetation N fixation in recent decades in some areas, such as eastern China and the central USA, which can relieve N limitations (Tian et al., 2022). Due to the scope of this paper, this issue is not addressed in this paper but is an important subject for further investigation to comprehensively understand the N limitation effect. Finally, this is an offline experiment in which the atmospheric forcing (such as downward radiation) is fixed. With a fixed atmospheric demand, the heat flux response due to the N limitation effect is also limited, as shown in section 4.1. A comprehensive assessment of the effect of N limitation on heat fluxes and atmospheric circulation needs to be conducted in a fully coupled atmosphere–land model.

Data availability. The evaluation/reference data sets from model data discussed in this paper are archived at https://doi.org/10.5281/zenodo.7196869

Code availability. The source code of biophysical-ecosystem-biogeochemical model, SSiB version5/TRIFFID/DayCent-SOM is archived at https://doi.org/10.5281/zenodo.7297108

Author contributions. ZX, YX, MH, and YL designed the coupling strategy between SSiB4/TRIFFID and DayCent-SOM. ZX conducted the simulation with suggestions from YX, WG, and WP. ZX, YX, and MH drafted the text and ZX made the figures. All authors (ZX, YX, WG, MH, YL and WP) have contributed to the analysis and the text.

Competing interests. The authors declare that they have no conflict of interest.

Acknowledgments. This study is supported by the National Science Foundation, Division of Atmospheric and Geospace Sciences (Grant No. AGS-1419526, AGS-1849654), and the Fundamental Research Funds for the Central Universities (Grant No. 14380172). The authors acknowledge the use of the Cheyenne supercomputer (https://doi.org/10.5065/D6RX99HX, Computational and Information Systems Laboratory, 2019), provided by NCAR CISL, for providing HPC resources. We also appreciate very comprehensive and constructive reviews by two anonymous reviewers, which greatly enhance this paper.

References

Aber, J. D., Goodale, C. L., Ollinger, S. V., Smith, M.-L., Magill, A. H., Martin, M. E., Hallett, R. A., and Stoddard, J. L.: Is nitrogen deposition altering the nitrogen status of northeastern forests?, Bioscience, 53, 375–389, https://doi.org/10.1641/0006-3568(2003)053[0375:INDATN]2.0.CO;2, 2003.

Aerts, R.: Nutrient Resorption from Senescing Leaves of Perennials: Are there General Patterns?, J. Ecol., 84, 597, https://doi.org/10.2307/2261481, 1996.

Ali, A. A., Xu, C., Rogers, A., McDowell, N. G., Medlyn, B. E., Fisher, R. A., Wullschleger, S. D., Reich, P. B., Vrugt, J. A., Bauerle, W. L., Santiago, L. S., and Wilson, C. J.: Global-scale environmental control of plant photosynthetic capacity, Ecol. Appl., 25, 2349–2365, https://doi.org/10.1890/14-2111.1, 2015.

Anav, A., Friedlingstein, P., Beer, C., Ciais, P., Harper, A., Jones, C., Murray-Tortarolo, G., Papale, D., Parazoo, N. C., Peylin, P., Wiltshire, A., and Zhao, M.: Spatiotemporal patterns of terrestrial gross primary production: A review, Rev. Geophys., 53, 785–818, https://doi.org/10.1002/2015RG000483, 2015.

Arora, V. K., Katavouta, A., Williams, R. G., Jones, C. D., Brovkin, V., Friedlingstein, P., Schwinger, J., Bopp, L., Boucher, O., Cadule, P., and Chamberlain, M. A.: Carbon – concentration and carbon – climate feedbacks in CMIP6 models and their comparison to CMIP5 models, 4173–4222, 2020.

Asaadi, A., Arora, V. K., and Arora, V. K.: Implementation of nitrogen cycle in the CLASSIC land model, Biogeosciences, 18, https://doi.org/10.5194/bg-18-669-2021, 2021.

Beer, C., Reichstein, M., Tomelleri, E., Ciais, P., Jung, M., Carvalhais, N., Rodenbeck, C., Arain, M. A., Baldocchi, D., Bonan, G. B., Bondeau, A., Cescatti, A., Lasslop, G., Lindroth, A., Lomas, M., Luyssaert, S., Margolis, H., Oleson, K. W., Roupsard, O., Veenendaal, E., Viovy, N., Williams, C., Woodward, F. I., and Papale, D.: Terrestrial Gross Carbon Dioxide Uptake: Global Distribution and Covariation with Climate, Science (80-.)., 329, 834–838, https://doi.org/10.1126/science.1184984, 2010.

Bonan, G. B.: Forests and Climate Change : Climate Benefits of Forests, Science (80-.)., 320, 1444–1449, 2008.

Bonan, G. B., Hartman, M. D., Parton, W. J., and Wieder, W. R.: Evaluating litter decomposition in earth system models with long-term litterbag experiments: An example using the Community Land Model version 4 (CLM4), Glob. Chang. Biol., 19, 957–974, https://doi.org/10.1111/gcb.12031, 2013.

Chen, X. and Chen, H. Y. H.: Plant mixture balances terrestrial ecosystem C:N:P stoichiometry, Nat. Commun., 12, https://doi.org/10.1038/s41467-021-24889-w, 2021.

Clarkson, D. T. and Hanson, J. B.: The Mineral Nutrition of Higher Plants, Annu. Rev. Plant Physiol., 31, 239–298, https://doi.org/10.1146/annurev.pp.31.060180.001323, 1980.

Collatz, G. J., Ball, J. T., Grivet, C., and Berry, J. A.: Physiological and environmental regulation of stomatal conductance, photosynthesis and transpiration: a model that includes a laminar boundary layer, Agric. For. Meteorol., 54, 107–136, https://doi.org/10.1016/0168-1923(91)90002-8, 1991.

Cox, P. M.: Description of the “TRIFFID” Dynamic Global Vegetation Model, Hadley Cent. Tech. Note-24, 2001.

Dan, L., Yang, X., Yang, F., Peng, J., Li, Y., Gao, D., Ji, J., and Huang, M.: Integration of nitrogen dynamics into the land surface model AVIM. Part 2: baseline data and variation of carbon and nitrogen fluxes in China, Atmos. Ocean. Sci. Lett., 13, https://doi.org/10.1080/16742834.2020.1819145, 2020.

Davies-Barnard, T., Meyerholt, J., Zaehle, S., Friedlingstein, P., Brovkin, V., Fan, Y., Fisher, R. A., Jones, C. D., Lee, H., Peano, D., Smith, B., Wärlind, D., and Wiltshire, A. J.: Nitrogen cycling in CMIP6 land surface models: Progress and limitations, Biogeosciences, 17, 5129–5148, https://doi.org/10.5194/bg-17-5129-2020, 2020.

Delpierre, N., Vitasse, Y., Chuine, I., Guillemot, J., Bazot, S., Rutishauser, T., and Rathgeber, C. B. K.: Temperate and boreal forest tree phenology: from organ-scale processes to terrestrial ecosystem models, https://doi.org/10.1007/s13595-015-0477-6, 2016.

Dorman, J. L. and Sellers, P. J.: A global climatology of albedo, roughness length and stomatal resistance for atmospheric general circulation models as represented by the Simple Biosphere Model (SiB), J. Appl. Meteorol., 28, 833–855, https://doi.org/10.1175/1520-0450(1989)028<0833:AGCOAR>2.0.CO;2, 1989.

Drewniak, B. and Gonzalez-Meler, M.: Earth System Model Needs for Including the Interactive Representation of Nitrogen Deposition and Drought Effects on Forested Ecosystems, Forests, 8, 267, https://doi.org/10.3390/f8080267, 2017.

Du, E., Terrer, C., Pellegrini, A. F. A., Ahlström, A., van Lissa, C. J., Zhao, X., Xia, N., Wu, X., and Jackson, R. B.: Global patterns of terrestrial nitrogen and phosphorus limitation, Nat. Geosci., 13, 221–226, https://doi.org/10.1038/s41561-019-0530-4, 2020.

Enquist, B., J. Brown, and G. West: Allometric scaling of plant energetics and population density. Nature, 395, 163{166, 1998.

Eyring, V., Bony, S., Meehl, G. A., Senior, C. A., Stevens, B., Stouffer, R. J., and Taylor, K. E.: Overview of the Coupled Model Intercomparison Project Phase 6 (CMIP6) experimental design and organization, Geosci. Model Dev., 9, 1937–1958, https://doi.org/10.5194/gmd-9-1937-2016, 2016.

Farquhar, G. D., von Caemmerer, S., and Berry, J. A.: A biochemical model of photosynthetic CO2 assimilation in leaves of C3 species, Planta, 149, 78–90, https://doi.org/10.1007/BF00386231, 1980.

Fisher, J. B., Sitch, S., Malhi, Y., Fisher, R. A., Huntingford, C., and Tan, S.-Y.: Carbon cost of plant nitrogen acquisition: A mechanistic, globally applicable model of plant nitrogen uptake, retranslocation, and fixation, Global Biogeochem. Cycles, 24, n/a-n/a, https://doi.org/10.1029/2009gb003621, 2010a.

Fisher, R., McDowell, N., Purves, D., Moorcroft, P., Sitch, S., Cox, P., Huntingford, C., Meir, P., and Ian Woodward, F.: Assessing uncertainties in a second-generation dynamic vegetation model caused by ecological scale limitations, New Phytol., 187, 666–681, https://doi.org/10.1111/j.1469-8137.2010.03340.x, 2010b.

Fleischer, K., Rammig, A., De Kauwe, M. G., Walker, A. P., Domingues, T. F., Fuchslueger, L., Garcia, S., Goll, D. S., Grandis, A., Jiang, M., Haverd, V., Hofhansl, F., Holm, J. A., Kruijt, B., Leung, F., Medlyn, B. E., Mercado, L. M., Norby, R. J., Pak, B., von Randow, C., Quesada, C. A., Schaap, K. J., Valverde-Barrantes, O. J., Wang, Y. P., Yang, X., Zaehle, S., Zhu, Q., and Lapola, D. M.: Amazon forest response to CO2 fertilization dependent on plant phosphorus acquisition, Nat. Geosci., 12, https://doi.org/10.1038/s41561-019-0404-9, 2019.

Foley, J. A., Levis, S., Prentice, I. C., Pollard, D., and Thompson, S. L.: Coupling dynamic models of climate and vegetation, Glob. Chang. Biol., 4, 561–579, https://doi.org/10.1046/j.1365-2486.1998.t01-1-00168.x, 1998.

Friedlingstein, P., Cox, P., Betts, R., Bopp, L., von Bloh, W., Brovkin, V., Cadule, P., Doney, S., Eby, M., Fung, I., Bala, G., John, J., Jones, C., Joos, F., Kato, T., Kawamiya, M., Knorr, W., Lindsay, K., Matthews, H. D., Raddatz, T., Rayner, P., Reick, C., Roeckner, E., Schnitzler, K.-G., Schnur, R., Strassmann, K., Weaver, A. J., Yoshikawa, C., and Zeng, N.: Climate–Carbon Cycle Feedback Analysis: Results from the C 4 MIP Model Intercomparison, J. Clim., 19, 3337–3353, https://doi.org/10.1175/JCLI3800.1, 2006.

Fu, Y. H., Piao, S., Delpierre, N., Hao, F., Hänninen, H., Geng, X., Peñuelas, J., Zhang, X., Janssens, I. A., and Campioli, M.: Nutrient availability alters the correlation between spring leaf-out and autumn leaf senescence dates, Tree Physiol., 39, https://doi.org/10.1093/treephys/tpz041, 2019.

Gerber, S., Hedin, L. O., Oppenheimer, M., Pacala, S. W., and Shevliakova, E.: Nitrogen cycling and feedbacks in a global dynamic land model, Global Biogeochem. Cycles, 24, 1–15, https://doi.org/10.1029/2008GB003336, 2010.

Ghimire, B., Riley, W. J., Koven, C. D., Mu, M., and Randerson, J. T.: Representing leaf and root physiological traits in CLM improves global carbon and nitrogen cycling predictions, J. Adv. Model. Earth Syst., 8, 598–613, https://doi.org/10.1002/2015MS000538, 2016.

Goll, D. S., Winkler, A. J., Raddatz, T., Dong, N., Colin Prentice, I., Ciais, P., and Brovkin, V.: Carbon-nitrogen interactions in idealized simulations with JSBACH (version 3.10), Geosci. Model Dev., 10, 2009–2030, https://doi.org/10.5194/gmd-10-2009-2017, 2017.

Gregory, J. M., Jones, C. D., Cadule, P., and Friedlingstein, P.: Quantifying carbon cycle feedbacks, J. Clim., 22, 5232–5250, https://doi.org/10.1175/2009JCLI2949.1, 2009.

Gristina, L., Scalenghe, R., García-Díaz, A., Matranga, M. G., Ferraro, V., Guaitoli, F., and Novara, A.: Soil organic carbon stocks under recommended management practices in different soils of semiarid vineyards, L. Degrad. Dev., 31, https://doi.org/10.1002/ldr.3339, 2020.

Del Grosso, S. J., Parton, W. J., Mosier, A. R., Ojima, D. S., Kulmala, A. E., and Phongpan, S.: General model for N 2 O and N 2 gas emissions from soils due to dentrification, Global Biogeochem. Cycles, 14, 1045–1060, https://doi.org/10.1029/1999GB001225, 2000.

Harper, A. B., Cox, P. M., Friedlingstein, P., Wiltshire, A. J., Jones, C. D., Sitch, S., Mercado, L. M., Groenendijk, M., Robertson, E., Kattge, J., Bönisch, G., Atkin, O. K., Bahn, M., Cornelissen, J., Niinemets, Ü., Onipchenko, V., Peñuelas, J., Poorter, L., Reich, P. B., Soudzilovskaia, N. A., and Van Bodegom, P.: Improved representation of plant functional types and physiology in the Joint UK Land Environment Simulator (JULES v4.2) using plant trait information, Geosci. Model Dev., 9, 2415–2440, https://doi.org/10.5194/gmd-9-2415-2016, 2016.

Heikkinen, J., Keskinen, R., Regina, K., Honkanen, H., and Nuutinen, V.: Estimation of carbon stocks in boreal cropland soils - methodological considerations, Eur. J. Soil Sci., 72, https://doi.org/10.1111/ejss.13033, 2021.

Herbert, D. A. and Fownes, J. H.: Phosphorus limitation of forest leaf area and net primary production on a highly weathered soil, Ecosystems, 29, 242–25, https://doi.org/10.1007/BF02186049, 1999.

Högberg, P., Näsholm, T., Franklin, O., and Högberg, M. N.: Tamm Review: On the nature of the nitrogen limitation to plant growth in Fennoscandian boreal forests, https://doi.org/10.1016/j.foreco.2017.04.045, 1 November 2017.

Hu, S., Chapin, F. S., Firestone, M. K., Field, C. B., and Chiariello, N. R.: Nitrogen limitation of microbial decomposition in a grassland under elevated CO 2, Nature, 409, 188–191, https://doi.org/10.1038/35051576, 2001.

Huang, H., Xue, Y., Li, F., and Liu, Y.: Modeling long-term fire impact on ecosystem characteristics and surface energy using a process-based vegetation-fire model SSiB4/TRIFFID-Fire v1.0, Geosci. Model Dev. Discuss., 1–41, https://doi.org/10.5194/gmd-2020-122, 2020.

Jung, M., Reichstein, M., and Bondeau, A.: Towards global empirical upscaling of FLUXNET eddy covariance observations: Validation of a model tree ensemble approach using a biosphere model, Biogeosciences, 6, 2001–2013, https://doi.org/10.5194/bg-6-2001-2009, 2009.

Jung, M., Reichstein, M., Margolis, H. A., Cescatti, A., Richardson, A. D., Arain, M. A., Arneth, A., Bernhofer, C., Bonal, D., Chen, J., Gianelle, D., Gobron, N., Kiely, G., Kutsch, W., Lasslop, G., Law, B. E., Lindroth, A., Merbold, L., Montagnani, L., Moors, E. J., Papale, D., Sottocornola, M., Vaccari, F., and Williams, C.: Global patterns of land-atmosphere fluxes of carbon dioxide, latent heat, and sensible heat derived from eddy covariance, satellite, and meteorological observations, J. Geophys. Res. Biogeosciences, 116, https://doi.org/10.1029/2010JG001566, 2011.

Kattge, J., Knorr, W., Raddatz, T., and Wirth, C.: Quantifying photosynthetic capacity and its relationship to leaf nitrogen content for global-scale terrestrial biosphere models, Glob. Chang. Biol., 15, 976–991, https://doi.org/10.1111/j.1365-2486.2008.01744.x, 2009.

Kolb, K. J. and Evans, R. D.: Implications of leaf nitrogen recycling on the nitrogen isotope composition of deciduous plant tissues, New Phytol., 156, 57–64, https://doi.org/10.1046/j.1469-8137.2002.00490.x, 2002.

Kou-Giesbrecht, S., Arora, V. K., Seiler, C., Arneth, A., Falk, S., Jain, A. K., Joos, F., Kennedy, D., Knauer, J., Sitch, S., O'sullivan, M., Pan, N., Sun, Q., Tian, H., Vuichard, N., and Zaehle, S.: Evaluating nitrogen cycling in terrestrial biosphere models: a disconnect between the carbon and nitrogen cycles, Earth Syst. Dyn., 14, https://doi.org/10.5194/esd-14-767-2023, 2023.

Lawrence, D. M., Fisher, R. A., Koven, C. D., Oleson, K. W., Swenson, S. C., Bonan, G., Collier, N., Ghimire, B., van Kampenhout, L., Kennedy, D., Kluzek, E., Lawrence, P. J., Li, F., Li, H., Lombardozzi, D., Riley, W. J., Sacks, W. J., Shi, M., Vertenstein, M., Wieder, W. R., Xu, C., Ali, A. A., Badger, A. M., Bisht, G., van den Broeke, M., Brunke, M. A., Burns, S. P., Buzan, J., Clark, M., Craig, A., Dahlin, K., Drewniak, B., Fisher, J. B., Flanner, M., Fox, A. M., Gentine, P., Hoffman, F., Keppel-Aleks, G., Knox, R., Kumar, S., Lenaerts, J., Leung, L. R., Lipscomb, W. H., Lu, Y., Pandey, A., Pelletier, J. D., Perket, J., Randerson, J. T., Ricciuto, D. M., Sanderson, B. M., Slater, A., Subin, Z. M., Tang, J., Thomas, R. Q., Val Martin, M., and

Zeng, X.: The Community Land Model Version 5: Description of New Features, Benchmarking, and Impact of Forcing Uncertainty, J. Adv. Model. Earth Syst., 11, 4245–4287, https://doi.org/10.1029/2018MS001583, 2019.

LeBauer, D. S. and Treseder, K. K.: Nitrogen Limitation of Net Primary Productivity In Terrestrial Ecosystems Is Globally Distributed, Ecology, 89, 371–379, https://doi.org/10.1890/06-2057.1, 2008.

Liu, Y., Xue, Y., Macdonald, G., Cox, P., and Zhang, Z.: Global vegetation variability and its response to elevated CO 2 , global warming, and climate variability - A study using the offline SSiB4/TRIFFID model and satellite data, Earth Syst. Dyn., 10, 9–29, https://doi.org/10.5194/esd-10-9-2019, 2019.

Liu, Y., Xue, Y., Li, Q., Lettenmaier, D., and Zhao, P.: Investigation of the Variability of Near-Surface Temperature Anomaly and Its Causes Over the Tibetan Plateau, J. Geophys. Res. Atmos., 125, https://doi.org/10.1029/2020JD032800, 2020.

Luke McCormack, M., Adams, T. S., Smithwick, E. A. H., and Eissenstat, D. M.: Variability in root production, phenology, and turnover rate among 12 temperate tree species, Ecology, 95, https://doi.org/10.1890/13-1942.1, 2014.

Lund, M., Falk, J. M., Friborg, T., Mbufong, H. N., Sigsgaard, C., Soegaard, H., and Tamstorf, M. P.: Trends in CO2 exchange in a high Arctic tundra heath, 2000-2010, J. Geophys. Res. Biogeosciences, 117, https://doi.org/10.1029/2011JG001901, 2012.

Ma, H.-Y., Mechoso, C. R., Xue, Y., Xiao, H., Neelin, J. D., and Ji, X.: On the connection between continental-scale land surface processes and the tropical climate in a coupled ocean-atmosphere-land system, J. Clim., 26, 9006–9025, https://doi.org/10.1175/JCLI-D-12-00819.1, 2013.

MacDonald, J. A., Dise, N. B., Matzner, E., Armbruster, M., Gundersen, P., and Forsius, M.: Nitrogen input together with ecosystem nitrogen enrichment predict nitrate leaching from European forests, Glob. Chang. Biol., 8, 1028–1033, https://doi.org/10.1046/j.1365-2486.2002.00532.x, 2002.

Makino, A. and Osmond, B.: Effects of Nitrogen Nutrition on Nitrogen Partitioning between Chloroplasts and Mitochondria in Pea and Wheat, Plant Physiol., 96, 355–362, https://doi.org/10.1104/pp.96.2.355, 1991.

Marmann, P., Wendler, R., Millard, P., and Heilmeier, H.: Nitrogen storage and remobilization in ash (Fraxinus excelsior) under field and laboratory conditions, Trees - Struct. Funct., 11, 298–305, https://doi.org/10.1007/s004680050088, 1997.

May, J. D. and Killingbeck, K. T.: Effects of preventing nutrient resorption on plant fitness and foliar nutrient dynamics, Ecology, 73, 1868–1878, https://doi.org/10.2307/1940038, 1992.

McDowell, N., Pockman, W. T., Allen, C. D., Breshears, D. D., Cobb, N., Kolb, T., Plaut, J., Sperry, J., West, A., Williams, D. G., Williams, D. G., and Yepez, E. A.: Mechanisms of plant survival and mortality during drought: Why do some plants survive while others succumb to drought?, New Phytol., 178, 719–739, https://doi.org/10.1111/j.1469-8137.2008.02436.x, 2008.

McGroddy, M. E., Daufresne, T., and Hedin, L. O.: Scaling of C:N:P stoichiometry in forests worldwide: Implications of terrestrial redfield-type ratios, https://doi.org/10.1890/03-0351, 2004.

Medlyn, B. E., Zaehle, S., De Kauwe, M. G., Walker, A. P., Dietze, M. C., Hanson, P. J., Hickler, T., Jain, A. K., Luo, Y., Parton, W., Oren, R., and Norby, R. J.: Using ecosystem experiments to improve vegetation models, Nat. Clim. Chang., 5, 528–534, https://doi.org/10.1038/nclimate2621, 2015.

Meyer-Grünefeldt, M., Calvo, L., Marcos, E., Von Oheimb, G., and Härdtle, W.: Impacts of drought and nitrogen addition on Calluna heathlands differ with plant life-history stage, J. Ecol., 103, 1141–1152, https://doi.org/10.1111/1365-2745.12446, 2015.

Meyerholt, J., Sickel, K., and Zaehle, S.: Ensemble projections elucidate effects of uncertainty in terrestrial nitrogen limitation on future carbon uptake, Glob. Chang. Biol., 26, https://doi.org/10.1111/gcb.15114, 2020.

Millard, P.: Measurement of the remobilization of nitrogen for spring leaf growth of trees under field conditions, Tree Physiol., 14, 1049–1054, https://doi.org/10.1093/treephys/14.7-8-9.1049, 1994.

Morgan, J. B. and Connolly, E. L.: Plant - Soil Interactions : Nutrient Uptake, Nat. Educ. Knowl., 4, 2013.

Mueller, P., Ladiges, N., Jack, A., Schmiedl, G., Kutzbach, L., Jensen, K., and Nolte, S.: Assessing the long-term carbon-sequestration potential of the semi-natural salt marshes in the European Wadden Sea, Ecosphere, 10, https://doi.org/10.1002/ecs2.2556, 2019.

Murray-Tortarolo, G., Anav, A., Friedlingstein, P., Sitch, S., Piao, S., Zhu, Z., Poulter, B., Zaehle, S., Ahlström, A., Lomas, M., Viovy, N., and Zeng, N.: Evaluation of land surface models in reproducing satellite-derived LAI over the high-latitude northern hemisphere. Part I: Uncoupled DGVMs, Remote Sens., 5, 4819–4838, https://doi.org/10.3390/rs5104819, 2013.

Neilsen, D., Millard, P., Neilsen, G. H., and Hogue, E. J.: Sources of N for leaf growth in a high-density apple (Malus domestica) orchard irrigated with ammonium nitrate solution, Tree Physiol., 17, 733–739, https://doi.org/10.1093/treephys/17.11.733, 1997.

Oleson, K. W., Lawrence, D. M., Bonan, G. B., Drewniak, B., Huang, M., Charles, D., Levis, S., Li, F., Riley, W. J., Zachary, M., Swenson, S. C., Thornton, P. E., Bozbiyik, A., Fisher, R., Heald, C. L., Kluzek, E., Lamarque, F., Lawrence, P. J., Leung, L. R., Muszala, S., Ricciuto, D. M., and Sacks, W.: Technical description of version 4.5 of the Community Land Model (CLM), NCAR Technical Note NCAR/TN-503+STR, Natl. Cent. Atmos. Res. Boulder, CO, 420pp, https://doi.org/DOI: 10.5065/D6RR1W7M, 2013.

Oliveira, D. C. de, Oliveira, D. M. da S., Freitas, R. de C. A. de, Barreto, M. S., Almeida, R. E. M. de, Batista, R. B., and Cerri, C. E. P.: Depth assessed and up-scaling of single case studies might overestimate the role of C sequestration by pastures in the commitments of Brazil's low-carbon agriculture plan, Carbon Manag., 12, https://doi.org/10.1080/17583004.2021.1977390, 2021.

Parton, W., Silver, W. L., Burke, I. C., Grassens, L., Harmon, M. E., Currie, W. S., King, J. Y., Adair, E. C., Brandt, L. A., Hart, S. C., and Fasth, B.: Global-scale similarities in nitrogen release patterns during long-term decomposition, Science (80-.)., 315, 361–364, https://doi.org/10.1126/science.1134853, 2007.

Parton, W. J., Scurlock, J. M. O., Ojima, D. S., Gilmanov, T. G., Scholes, R. J., Schimel, D. S., Kirchner, T., Menaut, J.-C., Seastedt, T., Garcia Moya, E., Kamnalrut, A., and Kinyamario, J. I.: Observations and modeling of biomass and soil organic matter dynamics for the grassland biome worldwide, Global Biogeochem. Cycles, 7, 785–809, https://doi.org/10.1029/93GB02042, 1993.

Parton, W. J., Ojima, D. S., Cole, C. V., and Schimel, D. S.: A general model for soil organic matter dynamics: sensitivity to litter chemistry, texture and management, Quant. Model. soil Form. Process. Proc. Symp. Minneapolis, 1992, 1994.

Parton, W. J., Hartman, M., Ojima, D., and Schimel, D.: DAYCENT and its land surface submodel: description and testing, Glob. Planet. Change, 19, 35–48, https://doi.org/10.1016/S0921-8181(98)00040-X, 1998.

Parton, W. J., Hanson, P. J., Swanston, C., Torn, M., Trumbore, S. E., Riley, W., and Kelly, R.: ForCent model development and testing using the Enriched Background Isotope Study experiment, J. Geophys. Res. Biogeosciences, 115, 1–15, https://doi.org/10.1029/2009JG001193, 2010.

Pastorello, G., Trotta, C., Canfora, E., Chu, H., Christianson, D., Cheah, Y. W., Poindexter, C., Chen, J., Elbashandy, A., Humphrey, M., Isaac, P., Polidori, D., Ribeca, A., van Ingen, C., Zhang, L., Amiro, B., Ammann, C., Arain, M. A., Ardö, J., Arkebauer, T., Arndt, S. K., Arriga, N., Aubinet, M., Aurela, M., Baldocchi, D., Barr, A., Beamesderfer, E., Marchesini, L. B., Bergeron, O., Beringer, J., Bernhofer, C., Berveiller, D., Billesbach, D., Black, T. A., Blanken, P. D., Bohrer, G., Boike, J., Bolstad, P. V., Bonal, D., Bonnefond, J. M., Bowling, D. R., Bracho, R., Brodeur, J., Brümmer, C., Buchmann, N., Burban, B., Burns, S. P., Buysse, P., Cale, P., Cavagna, M., Cellier, P., Chen, S., Chini, I., Christensen, T. R., Cleverly, J., Collalti, A., Consalvo, C., Cook, B. D., Cook, D., Coursolle, C., Cremonese, E., Curtis, P. S., D'Andrea, E., da Rocha, H., Dai, X., Davis, K. J., De Cinti, B., de Grandcourt, A., De Ligne, A., De Oliveira, R. C., Delpierre, N., Desai, A. R., Di Bella, C. M., di Tommasi, P., Dolman, H., Domingo, F., Dong, G., Dore, S., Duce, P., Dufrêne, E., Dunn, A., Dušek, J., Eamus, D., Eichelmann, U., ElKhidir, H. A. M., Eugster, W., Ewenz, C. M., Ewers, B., Famulari, D., Fares, S., Feigenwinter, I., Feitz, A., Fensholt, R., Filippa, G., Fischer, M., Frank, J., Galvagno, M., Gharun, M., Gianelle, D., et al.: The FLUXNET2015 dataset and the ONEFlux processing pipeline for eddy covariance data, Sci. data, 7, https://doi.org/10.1038/s41597-020-0534-3, 2020.

Peng, J., Wang, Y. P., Houlton, B. Z., Dan, L., Pak, B., and Tang, X.: Global Carbon Sequestration Is Highly Sensitive to Model-Based Formulations of Nitrogen Fixation, Global Biogeochem. Cycles, 34, https://doi.org/10.1029/2019GB006296, 2020.

Peñuelas, J., Poulter, B., Sardans, J., Ciais, P., Van Der Velde, M., Bopp, L., Boucher, O., Godderis, Y., Hinsinger, P., Llusia, J., Nardin, E., Vicca, S., Obersteiner, M., and Janssens, I. A.: Human-induced nitrogen-phosphorus imbalances alter natural and managed ecosystems across the globe, Nat. Commun., 4, https://doi.org/10.1038/ncomms3934, 2013.

Piao, S., Liu, Q., Chen, A., Janssens, I. A., Fu, Y., Dai, J., Liu, L., Lian, X., Shen, M., and Zhu, X.: Plant phenology and global climate change: Current progresses and challenges, https://doi.org/10.1111/gcb.14619, 2019.

Raddatz, T. J., Reick, C. H., Knorr, W., Kattge, J., Roeckner, E., Schnur, R., Schnitzler, K. G., Wetzel, P., and Jungclaus, J.: Will the tropical land biosphere dominate the climate-carbon cycle feedback during the twenty-first century?, Clim. Dyn., 29, 565–574, https://doi.org/10.1007/s00382-007-0247-8, 2007.

Reed, S. C., Yang, X., and Thornton, P. E.: Incorporating phosphorus cycling into global modeling efforts: A worthwhile, tractable endeavor, New Phytol., 208, https://doi.org/10.1111/nph.13521, 2015.

Reich, P. B., Hobbie, S. E., Lee, T., Ellsworth, D. S., West, J. B., Tilman, D., Knops, J. M. H., Naeem, S., and Trost, J.: Nitrogen limitation constrains sustainability of ecosystem response to CO2, Nature, 440, 922–925, https://doi.org/10.1038/nature04486, 2006.

Reich, P. B., Tjoelker, M. G., Pregitzer, K. S., Wright, I. J., Oleksyn, J., and Machado, J. L.: Scaling of respiration to nitrogen in leaves, stems and roots of higher land plants, Ecol. Lett., 11, 793–801, https://doi.org/10.1111/j.1461-0248.2008.01185.x, 2008.

Richardson, A. D., Anderson, R. S., Arain, M. A., Barr, A. G., Bohrer, G., Chen, G., Chen, J. M., Ciais, P., Davis, K. J., Desai, A. R., Dietze, M. C., Dragoni, D., Garrity, S. R., Gough, C. M., Grant, R., Hollinger, D. Y., Margolis, H. A., Mccaughey, H., Migliavacca, M., Monson, R. K., Munger, J. W., Poulter, B., Raczka, B. M., Ricciuto, D. M., Sahoo, A. K., Schaefer, K., Tian, H., Vargas, R., Verbeeck, H., Xiao, J., and Xue, Y.: Terrestrial biosphere models need better representation of vegetation phenology: Results from the North American Carbon Program Site Synthesis, Glob. Chang. Biol., 18, https://doi.org/10.1111/j.1365-2486.2011.02562.x, 2012.

Rogers, A.: The use and misuse of V(c,max) in Earth System Models., Photosynth. Res., 119, 15–29, https://doi.org/10.1007/s11120-013-9818-1, 2014.

Sardans, J., Rivas-Ubach, A., and Peñuelas, J.: The C:N:P stoichiometry of organisms and ecosystems in a changing world: A review and perspectives, https://doi.org/10.1016/j.ppees.2011.08.002, 2012.

Sellers, P. J., Mintz, Y., Sud, Y. C., and Dalcher, A.: A Simple Biosphere Model (SIB) for Use within General Circulation Models, J. Atmos. Sci., 43, 505–531, https://doi.org/10.1175/1520-0469(1986)043<0505:ASBMFU>2.0.CO;2, 1986.

Sheffield, J., Goteti, G., and Wood, E. F.: Development of a 50-year high-resolution global dataset of meteorological forcings for land surface modeling, J. Clim., 19, 3088–3111, https://doi.org/10.1175/JCLI3790.1, 2006.

Sitch, S., Prentice, I. C., Arneth, A., Bondeau, A., Cramer, W., Kaplan, J. O., Levis, S., Lucht, W., Sykes, M. T., Thonicke, K., and Venevsky, S.: Evaluation of ecosystem dynamics, plant geography and terrestrial carbon cycling in the LPJ dynamic global vegetation model, Glob. Chang. Biol., 9, 161–185, https://doi.org/10.1046/j.1365-2486.2003.00569.x, 2003.

Smith, B., Wärlind, D., Arneth, A., Hickler, T., Leadley, P., Siltberg, J., and Zaehle, S.: Implications of incorporating N cycling and N limitations on primary production in an individual-based dynamic vegetation model, Biogeosciences, 11, 2027–2054, https://doi.org/10.5194/bg-11-2027-2014, 2014.

Smith, S. V.: Stoichiometry of C:N:P Fluxes in Shallow-Water Marine Ecosystems, in: Comparative Analyses of Ecosystems, https://doi.org/10.1007/978-1-4612-3122-6_13, 1991.

Stenberg, J. A. and Muola, A.: How should plant resistance to herbivores be measured?, https://doi.org/10.3389/fpls.2017.00663, 2017.

Sterner, R. . and Elser, J. .: Ecological Stoichiometry: The Biology of Elements from Molecules to the Biosphere: Robert W. Sterner, James J. Elser, Peter Vitousek, 2002.

Sun, S. and Xue, Y.: Implementing a New Snow Scheme in Simplified Simple Biosphere Model, Adv. Atmos. Sci., 18, https://doi.org/10.1007/bf02919314, 2001.

Talhelm, A. F., Pregitzer, K. S., and Burton, A. J.: No evidence that chronic nitrogen additions increase photosynthesis in mature sugar maple forests, Ecol. Appl., 21, 2413–2424, https://doi.org/10.1890/10-2076.1, 2011.

Talmy, D., Blackford, J., Hardman-Mountford, N. J., Polimene, L., Follows, M. J., and Geider, R. J.: Flexible C : N ratio enhances metabolism of large phytoplankton when resource supply is intermittent, Biogeosciences, 11, https://doi.org/10.5194/bg-11-4881-2014, 2014.

Thomas, R. Q., Brookshire, E. N. J., and Gerber, S.: Nitrogen limitation on land: How can it occur in Earth system models?, Glob. Chang. Biol., 21, 1777–1793, https://doi.org/10.1111/gcb.12813, 2015.

Thum, T., Caldararu, S., Engel, J., Kern, M., Pallandt, M., Schnur, R., Yu, L., and Zaehle, S.: A new model of the coupled carbon, nitrogen, and phosphorus cycles in the terrestrial biosphere (QUINCY v1.0; revision 1996), Geosci. Model Dev., 12, https://doi.org/10.5194/gmd-12-4781-2019, 2019.

Tian, H., Bian, Z., Shi, H., Qin, X., Pan, N., Lu, C., Pan, S., Tubiello, F. N., Chang, J., Conchedda, G., Liu, J., Mueller, N., Nishina, K., Xu, R., Yang, J., You, L., and Zhang, B.: History of anthropogenic Nitrogen inputs (HaNi) to the terrestrial biosphere: A 5arcmin resolution annual dataset from 1860 to 2019, Earth Syst. Sci. Data, 14, https://doi.org/10.5194/essd-14-4551-2022, 2022.

Vicca, S., Luyssaert, S., Peñuelas, J., Campioli, M., Chapin, F. S., Ciais, P., Heinemeyer, A., Högberg, P., Kutsch, W. L., Law, B. E., Malhi, Y., Papale, D., Piao, S. L., Reichstein, M., Schulze, E. D., and Janssens, I. A.: Fertile forests produce biomass more efficiently, Ecol. Lett., 15, 520–526, https://doi.org/10.1111/j.1461-0248.2012.01775.x, 2012.

Vitasse, Y., Ursenbacher, S., Klein, G., Bohnenstengel, T., Chittaro, Y., Delestrade, A., Monnerat, C., Rebetez, M., Rixen, C., Strebel, N., Schmidt, B. R., Wipf, S., Wohlgemuth, T., Yoccoz, N. G., and Lenoir, J.: Phenological and elevational shifts of plants, animals and fungi under climate change in the European Alps, Biol. Rev., 96, https://doi.org/10.1111/brv.12727, 2021.

Vitousek, P.: Nutrient Cycling and Nutrient Use Efficiency Author (s): Peter Vitousek Source : The American Naturalist , Vol . 119 , No . 4 (Apr ., 1982), pp . 553-572 Published by : The University of Chicago Press for The American Society of Naturalists Stable URL, 119, 553–572, 1982.

Vitousek, P. and Howarth, R.: Nitrogen limitation on land and in the sea: How can it occur?, Biogeochemistry, 13, 3646–3653, https://doi.org/10.1007/BF00002772, 1991.

Walker, A. P., Beckerman, A. P., Gu, L., Kattge, J., Cernusak, L. A., Domingues, T. F., Scales, J. C., Wohlfahrt, G., Wullschleger, S. D., and Woodward, F. I.: The relationship of leaf photosynthetic traits - Vcmax and Jmax - to leaf nitrogen, leaf phosphorus, and specific leaf area: A meta-analysis and modeling study, Ecol. Evol., 4, https://doi.org/10.1002/ece3.1173, 2014.

Wang, C. and Tang, Y.: Responses of plant phenology to nitrogen addition: a meta-analysis, Oikos, 128, https://doi.org/10.1111/oik.06099, 2019.

Wang M, Liu Y, Hao Z, Wang Y. Respiration rate of broadleaved Korean pine forest ecosystem in Changbai Mountains.. - Chin. J. Appl. Ecol. 2006,17(10) : 1789 ~ 1795.

Wang, Y. P., Law, R. M., and Pak, B.: A global model of carbon, nitrogen and phosphorus cycles for the terrestrial biosphere, Biogeosciences, 7, 2261–2282, https://doi.org/10.5194/bg-7-2261-2010, 2010.

Wiltshire, A., Burke, E., Chadburn, S., Jones, C., Cox, P., Davies-Barnard, T., Friedlingstein, P., Harper, A., Liddicoat, S., Sitch, S., and Zaehle, S.: JULES-CN: a coupled terrestrial Carbon-Nitrogen Scheme (JULES vn5.1), Geosci. Model Dev. Discuss., 1–40, https://doi.org/10.5194/gmd-2020-205, 2020.

Wingler, A., Purdy, S., MacLean, J. A., and Pourtau, N.: The role of sugars in integrating environmental signals during the regulation of leaf senescence, in: Journal of Experimental Botany, https://doi.org/10.1093/jxb/eri279, 2006.

Xiao, Z., Liang, S., Wang, J., Chen, P., Yin, X., Zhang, L., and Song, J.: Use of general regression neural networks for generating the GLASS leaf area index product from time-series MODIS surface reflectance, IEEE Trans. Geosci. Remote Sens., 52, 209–223, https://doi.org/10.1109/TGRS.2013.2237780, 2014.

Xue, Y., Sellers, P. J., Kinter, J. L., and Shukla, J.: A Simplified biosphere model for global climate studies, J. Clim., 4, 345–364, https://doi.org/10.1175/1520-0442(1991)004<0345:ASBMFG>2.0.CO;2, 1991.

Xue, Y., Zeng, F. J., and Schlosser, C. A.: SSiB and its sensitivity to soil properties-A case study using HAPEX-Mobilhy data, Glob. Planet. Change, 13, https://doi.org/10.1016/0921-8181(95)00045-3, 1996.

Xue, Y., Sellers, P. J., Zeng, F. J., and Schlosser, C. A.: Comments on "Use of midlatitude soil moisture and meteorological observations to validate soil moisture simulations with biosphere and bucket models," J. Clim., 10, https://doi.org/10.1175/1520-0442(1997)010<0374:COUOMS>2.0.CO;2, 1997.

Xue, Y., Juang, H.-M. H., Li, W.-P., Prince, S., DeFries, R., Jiao, Y., and Vasic, R.: Role of land surface processes in monsoon development: East Asia and West Africa, J. Geophys. Res. Atmos., 109, n/a-n/a, https://doi.org/10.1029/2003jd003556, 2004.

Xue, Y., De Sales, F., Vasic, R., Mechoso, C. R., Arakawa, A., and Prince, S.: Global and seasonal assessment of interactions between climate and vegetation biophysical processes: A GCM study with different land-vegetation representations, J. Clim., 23, 1411–1433, https://doi.org/10.1175/2009JCLI3054.1, 2010.

Xue, Y., Diallo, I., Boone, A. A., Yao, T., Zhang, Y., Zeng, X., Neelin, J. D., Lau, W. K. M., Pan, Y., Liu, Y., Pan, X., Tang, Q., Oevelen, P. J. van, Sato, T., Koo, M.-S., Materia, S., Shi, C., Yang, J., Ardilouze, C., Lin, Z., Qi, X., Nakamura, T., Saha, S. K., Senan, R., Takaya, Y., Wang, H., Zhang, H., Zhao, M., Nayak, H. P., Chen, Q., Feng, J., Brunke, M. A., Fan, T., Hong, S., Nobre, P., Peano, D., Qin, Y., Vitart, F., Xie, S., Zhan, Y., Klocke, D., Leung, R., Li, X., Ek, M., Guo, W., Balsamo, G., Bao, Q., Chou, S. C., Rosnay, P. de, Lin, Y., Zhu, Y., Qian, Y., Zhao, P., Tang, J., Liang, X.-Z., Hong, J., Ji, D., Ji, Z., Qiu, Y., Sugimoto, S., Wang, W., Yang, K., and Yu, M.: Spring Land Temperature in Tibetan Plateau and Global-Scale Summer Precipitation: Initialization and Improved Prediction, Bull. Am. Meteorol. Soc., 103, https://doi.org/10.1175/bams-d-21-0270.1, 2022.

Xue, Y., Diallo, I., Boone, A. A., Zhang, Y., Zeng, X., Lau, W. K. M., Neelin, J. D., Yao, T., Tang, Q., Sato, T., Koo, M. S., Vitart, F., Ardilouze, C., Saha, S. K., Materia, S., Lin, Z., Takaya, Y., Yang, J., Nakamura, T., Qi, X., Qin, Y., Nobre, P., Senan, R., Wang, H., Zhang, H., Zhao, M., Nayak, H. P., Pan, Y., Pan, X., Feng, J., Shi, C., Xie, S., Brunke, M. A., Bao, Q., Bottino, M. J., Fan, T., Hong, S., Lin, Y., Peano, D., Zhan, Y., Mechoso, C. R., Ren, X., Balsamo, G., Chou, S. C., de Rosnay, P., van Oevelen, P. J., Klocke, D., Ek, M., Li, X., Guo, W., Zhu, Y., Tang, J., Liang, X. Z., Qian, Y., and Zhao, P.: Remote effects of Tibetan Plateau spring land temperature on global subseasonal to seasonal precipitation prediction and comparison with effects of sea surface temperature: the GEWEX/LS4P Phase I experiment, Clim. Dyn., https://doi.org/10.1007/s00382-023-06905-5, 2023.

Yang, N., Zavišić, A., Pena, R., and Polle, A.: Phenology, photosynthesis, and phosphorus in european beech (Fagus sylvatica L.) in two forest soils with contrasting P contents, J. Plant Nutr. Soil Sci., 179, https://doi.org/10.1002/jpln.201500539, 2016.

Yang S, Wen S, Lin J and Yin Z. Respiration of non-photosynthetic organs of Korean pine in spring. -Chin.J. Appl. Ecol, 1992,3(4):386—388.

Yin, T. F., Zheng, L. L., Cao, G. M., Song, M. H., and Yu, F. H.: Species-specific phenological responses to long-term nitrogen fertilization in an alpine meadow, J. Plant Ecol., 10, https://doi.org/10.1093/jpe/rtw026, 2017.

Yu, L., Ahrens, B., Wutzler, T., Zaehle, S., and Schrumpf, M.: Modeling Soil Responses to Nitrogen and Phosphorus Fertilization Along a Soil Phosphorus Stock Gradient, Front. For. Glob. Chang., 3, https://doi.org/10.3389/ffgc.2020.543112, 2020.

Zaehle, S., Jones, C. D., Houlton, B., Lamarque, J. F., and Robertson, E.: Nitrogen availability reduces CMIP5 projections of twenty-first-century land carbon uptake, J. Clim., 28, 2494–2511, https://doi.org/10.1175/JCLI-D-13-00776.1, 2015.

Zhan, X., Xue, Y., and Collatz, G. J.: An analytical approach for estimating CO<inf>2</inf> and heat fluxes over the Amazonian region, Ecol. Modell., 162, 97–117, https://doi.org/10.1016/S0304-3800(02)00405-2, 2003.

Zhang, Z., Xue, Y., MacDonald, G., Cox, P. M., and Collatz, G. J.: Investigation of North American vegetation variability under recent climate: A study using the SSiB4/TRIFFID biophysical/dynamic vegetation model, J. Geophys. Res., 120, 1300–1321, https://doi.org/10.1002/2014JD021963, 2015.

Zhou, L., Zhou, W., Chen, J., Xu, X., Wang, Y., Zhuang, J., and Chi, Y.: Land surface phenology detections from multi-source remote sensing indices capturing canopy photosynthesis phenology across major land cover types in the Northern Hemisphere, Ecol. Indic., 135, https://doi.org/10.1016/j.ecolind.2022.108579, 2022.

Zhu, Q., Riley, W. J., Tang, J., Collier, N., Hoffman, F. M., Yang, X., and Bisht, G.: Representing Nitrogen, Phosphorus, and Carbon Interactions in the E3SM Land Model: Development and Global Benchmarking, J. Adv. Model. Earth Syst., 11, https://doi.org/10.1029/2018MS001571, 2019.

Zhu, Z., Bi, J., Pan, Y., Ganguly, S., Anav, A., Xu, L., Samanta, A., Piao, S., Nemani, R. R., and Myneni, R. B.: Global data sets of vegetation leaf area index (LAI)3g and fraction of photosynthetically active radiation (FPAR)3g derived from global inventory modeling and mapping studies (GIMMS) normalized difference vegetation index (NDVI3G) for the period 1981 to 2, Remote Sens., 5, 927–948, https://doi.org/10.3390/rs5020927, 2013.